PHILOSOPHICAL TRANSACTIONS A

royalsocietypublishing.org/journal/rsta

Research



Cite this article: Cassier M, DeGiovanni T, Guenneau S, Guevara Vasquez F. 2022 Active exterior cloaking for the two-dimensional Helmholtz equation with complex wavenumbers and application to thermal cloaking. *Phil. Trans. R. Soc. A* 380: 20220073. https://doi.org/10.1098/rsta.2022.0073

Received: 3 March 2022 Accepted: 9 May 2022

One contribution of 17 to a theme issue 'Wave generation and transmission in multi-scale complex media and structured metamaterials (part 2)'.

Subject Areas:

differential equations, integral equations, wave motion

Keywords:

Helmholtz equation, heat equation, active cloaking, potential theory, Green identities

Author for correspondence:

Fernando Guevara Vasquez e-mail: fguevara@math.utah.edu

Electronic supplementary material is available online at https://doi.org/10.6084/m9.figshare. c.6167566.

THE ROYAL SOCIETY PUBLISHING

Active exterior cloaking for the two-dimensional Helmholtz equation with complex wavenumbers and application to thermal cloaking

Maxence Cassier¹, Trent DeGiovanni², Sébastien Guenneau³ and Fernando Guevara Vasquez²

¹Institut Fresnel, CNRS, Centrale Marseille, Aix Marseille University, Marseille, France

²Mathematics Department, University of Utah, Salt Lake City, UT 84112, USA

³UMI 2004 Abraham de Moivre-CNRS, Imperial College London, London SW7 2AZ, UK

(b) SG, 0000-0002-5924-622X; FGV, 0000-0001-8746-3582

We design sources for the two-dimensional Helmholtz equation that can cloak an object by cancelling out the incident field in a region, without the sources completely surrounding the object to hide. As in previous work for real positive wavenumbers, the sources are also determined by the Green identities. The novelty is that we prove that the same approach works for complex wavenumbers which makes it applicable to a variety of media, including media with dispersion, loss and gain. Furthermore, by deriving bounds on Graf's addition formulas with complex arguments, we obtain new estimates that allow to quantify the quality of the cloaking effect. We illustrate our results by applying them to achieve active exterior cloaking for the heat equation.

This article is part of the theme issue 'Wave generation and transmission in multi-scale complex media and structured metamaterials (part 2)'.

1. Introduction

Our goal is to use specially designed sources to cloak or hide a bounded object from a probing field u_i satisfying

© 2022 The Author(s) Published by the Royal Society. All rights reserved.

$$\Delta u_i + k^2 u_i = 0, \tag{1.1}$$

in a region containing the object. Here Δ denotes the Laplacian. This is called *active cloaking* since to build the cloak, we use sources rather than passive materials that may be hard to manufacture [1]. Moreover, a great advantage of the cloaking strategy we present is that it does not require completely surrounding the object to hide it, hence the *exterior cloaking* name. This idea was introduced in [2] for the two-dimensional Helmholtz equation with k real (lossless propagative media). Here we allow k to take any values in the complex plane, except for the negative real axis. Thus, using a frequency decomposition of the transient regime via a Fourier–Laplace transform on the time variable, our approach applies to cloaking objects for acoustic waves propagating in passive, dissipative, active or dispersive media, and similarly for diffusive media. Interestingly, complex wavenumbers open a path to exterior cloaking for problems modelled by partial differential equations with second order derivatives in space and with time derivatives of an arbitrary order. Moreover, we derive new error estimates on the convergence of active exterior cloaking and apply our results to cloaking for the heat equation in the transient regime.

(a) Active exterior cloaking

From potential theory [3] or using the Green identities (e.g. [4]), it is possible to reproduce a solution to the Helmholtz equation inside of a bounded region Ω and getting, simultaneously, a zero field outside of Ω . This is achieved by a distribution of monopole and dipole sources on the boundary $\partial\Omega$ that can be expressed in terms of the value of the field and its normal derivative on $\partial\Omega$. As observed by Miller [5], this principle can be used for cloaking. Indeed the monopole and dipole distribution can be chosen to generate the *cloak field*

$$u_c = \begin{cases} -u_i & \text{in } \Omega \\ 0 & \text{outside } \overline{\Omega}, \end{cases}$$
 (1.2)

where \overline{X} denotes the closure of a set X. We see that by linearity, $u_c + u_i$ cancels out inside Ω without affecting u_i outside of Ω . The end result is that objects inside Ω will not scatter, and it is impossible to detect the cloaked field outside of Ω . We call this approach the *Green identity cloak*. A first drawback of this approach is that the probing field u_i needs to be known ahead of time. A second drawback is that the sources completely surround the object that we wish to hide. The exterior cloaking approach lifts this second limitation.

To achieve exterior cloaking, we follow the approach in [6] for the two-dimensional Helmholtz equation with real wavenumbers, see also [7] for the three-dimensional Helmholtz equation and [8,9] for elasticity. See also [10] for a general analysis. The key observation is that Graf's addition formulas (see e.g. §10.23 in [11] or [12]) can be used to move a monopole (or dipole) located at y to a new location x_j . However, the price to pay is that the new source is obtained by an infinite superposition of multipolar sources that diverges in the disc

$$D_{x_j,y} := \{ x \in \mathbb{R}^2 \mid |x - x_j| \le |y - x_j| \}, \tag{1.3}$$

where $|\cdot|$ denotes the Euclidean norm. By linearity, we should also be able to move a distribution of monopoles or dipoles on a compact portion $\partial \Omega_j$ of the boundary $\partial \Omega$ to a new location x_j , obtaining the same cloak field u_c , provided we are outside of the closed disc

$$R_{j} = \{ x \in \mathbb{R}^{2} \mid |x - x_{j}| \le \max_{y \in \partial \Omega_{j}} |y - x_{j}| \}.$$
 (1.4)

Assuming the portions $\partial \Omega_j$ cover $\partial \Omega$ and their intersection is reduced to points, we can achieve the same cloaking effect as the Green identity cloak if we are outside of the region $R_1 \cup R_2 \cup ... \cup$

Phil. Trans. R. Soc. A 380: 2022007:

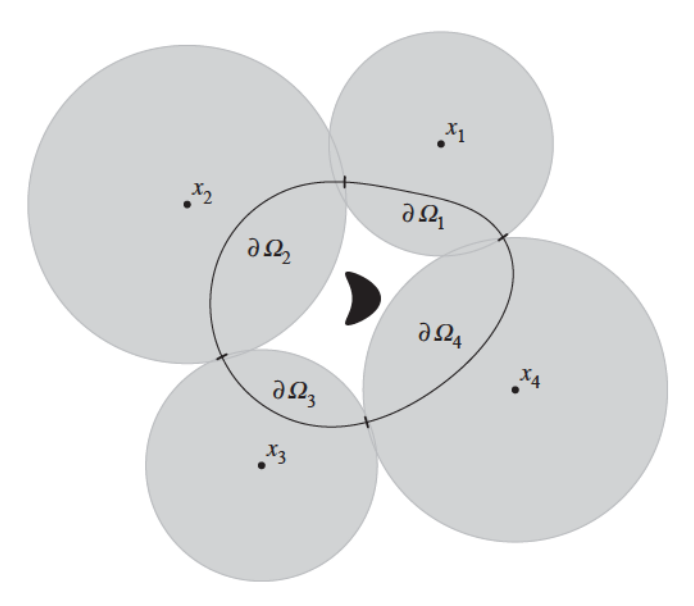


Figure 1. Active exterior cloak for the Helmholtz equation starting from the Green identities applied on the surface $\partial \Omega$ of a domain Ω . To hide the object (kite) inside Ω , the sources in the portions $\partial \Omega_j$ of $\partial \Omega$ are moved to new locations x_j , $j=1,\ldots,N_{\text{dev}}$. The grey discs are the domains of divergence R_j for the new fields, see (1.4). For illustration purposes, we took $N_{\text{dev}}=4$, but three sources would suffice to achieve exterior cloaking.

 $R_{N_{\text{dev}}}$ (see figure 1 for an illustration). Here we extend this approach to complex wavenumbers that enables new applications. Moreover, by obtaining bounds for the Graf's addition formula with complex arguments, we derive a simple geometric series ansatz to predict the truncation error for the field generated by the multipolar sources. This extends previous work on the truncation error of Graf's addition formulae [13,14] for real arguments. The truncation estimates allow us to quantitatively predict the quality of the cloaking effect.

(b) Extending active exterior cloaking to complex *k*

Many partial differential equations in the frequency domain lead to the Helmholtz equation with a complex wavenumber. To name a few: the telegraph equation, the diffusion equation, Schrödinger equation and the Klein–Gordon equation (e.g. [15,16] or [17], §1.1.2). More generally, consider partial differential equations (PDEs) in the time domain of the form

$$P(\partial_t)\mathfrak{u} = \Delta\mathfrak{u} + \mathfrak{f},\tag{1.5}$$

where P is a polynomial of degree n and f(x,t) is a source term. Since (1.5) is a constant coefficient PDE, it admits a solution in the distributional sense, for example for any compactly supported source term \mathfrak{f} . This can be seen from the Malgrange–Ehrenpreis theorem, though without uniqueness or causality guarantees, e.g. [18].

Many classic equations are of the form (1.5). For example, the wave equation can be obtained with $P(z) = z^2$, and the heat equation with P(z) = z. For a *causal* source \mathfrak{f} (i.e. $\mathfrak{f}(x,t) = 0$ for t < 0), we can analyse equations of the form (1.5) in the frequency domain by means of the Fourier–Laplace transform

$$u(x,\omega) = \int_0^\infty dt \, e^{i\omega t} u(x,t), \tag{1.6}$$

where ω is in general complex and $\mathfrak u$ is assumed to grow sufficiently slowly. For example, we may assume that $\mathfrak u(x,t)$ satisfies for t>0

$$||\mathfrak{u}(\cdot,t)|| < C e^{\alpha t} (1+t^p),$$
 (1.7)

where C > 0, $p \in \mathbb{N}$ and $\alpha \in \mathbb{R}$ are constants, e.g. [15,19]. Under this assumption, the Fourier–Laplace transform is defined on the half plane

$$\mathbb{C}_{\alpha}^{+} := \{ \omega \in \mathbb{C} \mid \operatorname{Im}(\omega) > \alpha \}. \tag{1.8}$$

The choice of norm depends on the spatial differential operator. Since we focus on the Laplacian, we use the H^1 norm on any bounded open set of interest (α, p, C) could depend on the choice of the set). To summarize, in our situation, we may assume that $\mathfrak{u} \in L^1_{loc}((0,\infty),H^1_{loc}(\mathbb{R}^2))^1$ satisfies the growth condition (1.7) for the H^1 -norm on any bounded open set of \mathbb{R}^2 . Furthermore, we assume that all its time derivatives up to order n (the degree of the polynomial P) and the source term \mathfrak{f} are in $L^1_{loc}((0,\infty),L^2_{loc}(\mathbb{R}^2))$ and satisfy (1.7) on any bounded open set of \mathbb{R}^2 for the L^2 -norm (with the same real α as for \mathfrak{u} , that could depend only on the spatial set). This growth condition allows to make sense of the Fourier–Laplace transform for solutions that may grow exponentially in time, L^2 as is the case of active media.

Remark 1.1. The Fourier–Laplace transform is equivalent to the Laplace transform with $s=-\mathrm{i}\omega$ (see e.g. (4.5) for a definition). Here we choose this convention because when ω is real it corresponds to the angular frequency in wave propagation.

Assuming $\mathfrak u$ and all its time derivatives up to order n-1 vanish at t=0, we get that $u(x,\omega)$ satisfies the inhomogeneous Helmholtz equation:

$$\Delta u + k^2 u = -f,\tag{1.9}$$

with the relation $k^2 = -P(-i\omega)$. This formalism shows that k may be complex, e.g. in the case of the heat equation. Another example is the modified wave equation with $P(z) = z^2 + \alpha z$, $\alpha \in \mathbb{R}$. If $\alpha > 0$, this is the dissipative wave equation which corresponds to wave propagation in lossy media. If $\omega > 0$, we can choose the root k such that Im(k) > 0 to get spatially decreasing solutions to (1.9).⁴ Whereas with $\alpha < 0$, $\omega > 0$ we choose k such that Im(k) < 0 to get spatially increasing solutions corresponding to an amplifying medium (medium with gain) (e.g. [25]). We summarize the possibilities in figure 2. We have highlighted the region with $Re(k^2) < 0$ (or equivalently |Re(k)| < |Im(k)|), since a form of the maximum principle holds for the Helmholtz equation with such k [26,27]. Later in §3b, we see that the maximum principle gives a form of stability for the accuracy of approximations to our cloaking approach.

Other situations where complex wavenumber k arises are in passive, dispersive media, where the index of refraction is a complex valued function of frequency ω [28–33]. A typical example is the dispersion law given by the Drude–Lorentz model in electromagnetism, which can model both metals and metamaterials with negative index of refraction [34]. In acoustics (see e.g. section 1.1.2 of [17]), complex wavenumbers also arise when studying acoustic (pressure) waves propagating within complex (but homogeneous and isotropic) fluids (i.e. not barotropic) with a relaxation time (due to the presence of solid particles or bubbles) that can be modelled in the time-harmonic regime with $k^2 = \omega^2/(c^2(1-i\omega\tau_p))$. Here c is the speed of sound (m s⁻¹), ω the pulsation frequency (rad s⁻¹) and τ_p the density relaxation time (s).

We note that the frequency domain formulation gives a strategy for active exterior cloaking in the time domain for equations of the form (1.5), and even when the powers are fractional or negative (which corresponds to integro-differential equations). One caveat of our approach is that

¹Let $X \subset \mathbb{R}^d$. We recall that for $p \ge 1$, $L_{loc}^p(X)$ (resp. H_{loc}^1) is the set of functions that are L^p (resp. H^1) on any bounded open subset of X, with closure inside X. See [20,21].

²The growth condition (1.6) and the regularity assumption $\mathfrak{u} \in L^1_{loc}((0,\infty),L^2_{loc}(\mathbb{R}^2))$ ensure in particular the existence of the Laplace transform (1.6) as a Bochner integral with respect to t valued in L^2 [19], and thus also pointwise for almost all $x \in \mathbb{R}^2$ and all $\omega \in \mathbb{C}^+_{\alpha}$. We point out that in a more general context, the Fourier–Laplace transform can be extended to spaces of distributions, e.g. [15,22,23].

³By 'active media', we mean there is energy input that may lead to increase of the magnitude of the fields in time, see for instance [24]. By 'gain media', we mean that there are spatially growing outgoing solutions of the Helmholtz equation as e.g. resonant states, see [25]. This is not a universal nomenclature.

⁴We shall see in §2 that the decay is consistent with the choice of Green function (2.1).

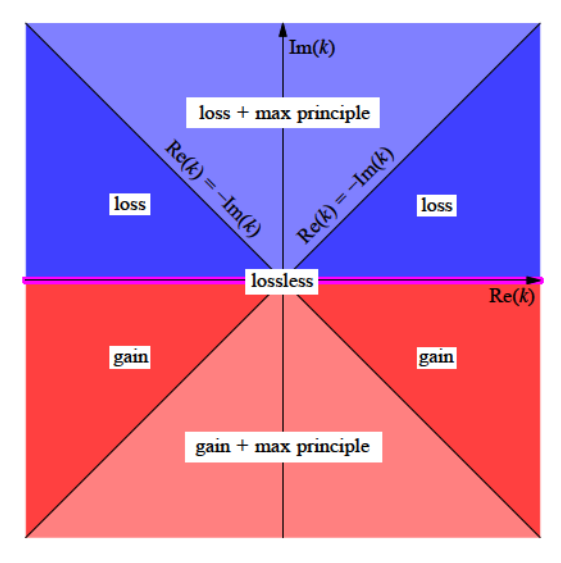


Figure 2. Diagram of cases for the wavenumber k defined by $k = \pm i\sqrt{P(-i\omega)}$, where we used the principal square root and the sign is chosen to match the sign of Im(k). When Im(k) = 0 we have $k = \pm \sqrt{-P(-i\omega)}$. (Online version in colour.)

the sources need to make sense physically in (1.5). However, for active thermal cloaking (§4) the sources we obtain can be thought of as Peltier devices [35].

(c) Structure of the paper

We derive convergence estimates for the Graf addition formula applied to Green functions in §2, showing that the truncation error of the series can be dominated by that of a geometric series with ratio that depends only on the position of the evaluation point relative to the positions of the original and new sources. This result can be applied to get truncation estimates for the multipolar source expansions that appear in active exterior cloaking for possibly complex wavenumbers (§3). In §3, we also use a form of the maximum principle for the Helmholtz equation, which guarantees the truncation errors in a region are maximum on the boundary of the region (this only holds for a class of dissipative or diffusive media). The time domain problem for the heat equation is then considered in §4. We conclude with some future work and perspectives in §5.

2. Moving sources

The field evaluated at *x* corresponding to a point source located at *y* is given by the appropriate Green function

$$G(x - y; k) = \frac{i}{4} H_0^{(1)}(k|x - y|), \tag{2.1}$$

where $H_0^{(1)}$ is the zeroth-order Hankel function of the first kind, 5 (e.g. [11], eqn 10.4.3). Moreover, $G(x;k) \to 0$ as $|x| \to \infty$ whenever $\operatorname{Im}(k) \ge 0$, as can be seen from the large argument asymptotics for Bessel functions ([11], eqn 10.2.5). When $\operatorname{Im}(k) < 0$, the same asymptotic shows that $|G(x;k)| \to \infty$. Thus, the choice of Green function is consistent with the loss and gain conventions in the diagram appearing in figure 2.

⁵In the context of the wave equation with constant propagation speed c, we have $k = \omega/c > 0$ and the choice of Green function (2.1) corresponds to outgoing waves. This is consistent with the Fourier–Laplace transform convention (1.6) and with the convention that the corresponding time harmonic field is $\text{Re}(\exp[-i\omega t]G(x-y;k))$. In fact Re(k) > 0 also gives outgoing waves, as can be seen e.g. from adapting the discussion ([17], eqn 1.2.12) from three- to two-dimensional using ([11], eqn 10.4.3).

Thanks to the Graf addition formulae ([11], eqn 10.23.7), we can move (with three significant caveats) the source from location y to another location x_i , indeed:

$$G(x-y;k) = \frac{i}{4} \sum_{m=-\infty}^{\infty} H_m^{(1)}(k|x-x_j|) J_m(k|y-x_j|) \exp[im\theta],$$
 (2.2)

where $\theta = \arg(x - x_j) - \arg(y - x_j)$ and $\arg x$ is the counter-clockwise angle between the vectors x and (1,0). Here J_m is the mth-order Bessel function of the first kind, e.g. ([11], eqn 10.2.2). The first caveat is that the new source in (2.2) is no longer a monopole point source like (2.1), but a linear combination of Helmholtz equation solutions that diverge as $|x - x_j| \to 0$, of the form $V_m(x - x_j)$ where

$$V_m(x) = \exp[im \arg(x)] H_m^{(1)}(k|x|), \tag{2.3}$$

and that are known as *multipolar sources* (or *cylindrical outgoing waves* when k is real). The second caveat is that the Graf addition formula is only valid for $k \in \mathbb{C} \setminus (-\infty, 0]$. The third caveat is that the series converges only outside of the disc $D_{x_i,y}$, as defined in (1.3).

The same method and caveats apply if we desire to move a dipole located at y and oriented in the direction v(y) normal to the boundary $\partial \Omega$ at y, or more precisely

$$\frac{\partial G}{\partial \nu(y)}(x-y;k) = \frac{i}{4} \sum_{m=-\infty}^{\infty} H_m^{(1)}(k|x-x_j|) \frac{\partial}{\partial \nu(y)} (J_m(k|y-x_j|) \exp[im\theta]), \tag{2.4}$$

where θ is the same as in (2.2). Formally speaking, equation (2.4) can be obtained by taking the gradient term by term (with respect to y) in (2.2) and then taking the dot product with v(y). The differentiation term by term can be easily justified by using lemma 2.2 in order to prove that the involved series of gradients is locally normally convergent (and thus locally uniformly convergent) with respect to y when x, x_i are fixed.

We start in §2a by proving convergence estimates for (2.2) and (2.4). The convergence errors are illustrated numerically in §2b.

(a) Truncation error estimates

To study the convergence rate of (2.2) and (2.4) we define the truncation to 2M + 1 terms of the formula (2.2) for moving the point source at x_i to location y by

$$G_{j,M}(x-y;k) = \frac{i}{4} \sum_{m=-M}^{M} H_m^{(1)}(k|x-x_j|) J_m(k|y-x_j|) \exp[im\theta],$$
 (2.5)

where M is an integer. The truncation error for a monopole and dipole are given, respectively, by

$$R_{j,M}(x;k) = |G(x-y;k) - G_{j,M}(x-y;k)| R'_{j,M}(x;k) = \left| \frac{\partial}{\partial \nu(y)} [G(x-y;k) - G_{j,M}(x-y;k)] \right|.$$
 (2.6)

and

Downloaded from https://royalsocietypublishing.org/ on 03 August 2023 by Fernando Vasquez

Here v(y) can be the normal to the boundary $\partial\Omega$ or any other unit length vector. In the next theorem, we show that these truncation errors are dominated by the truncation errors of well-known series such as geometric series. Our convergence estimates account for moving sources from different original positions y to a single new position x_j . The case of different original positions y is useful in the context of active exterior cloaking (§3). We point out that the monopole truncation error was derived for real wavenumbers by ([13], Lemma 9) and [14], using techniques that are similar to the ones we use here. Theorem 2.1 applies to the monopole and the dipole truncation errors and allows for estimates that are *uniform* with respect to original source location y, evaluation point x and complex wavenumbers k.

Theorem 2.1. Let $x_i \in \mathbb{R}^2$, $M \ge 2$, $Y \subset \mathbb{R}^2$ be a compact set and define the disc

$$D_j^{\max} = \{x \in \mathbb{R}^2 \mid |x - x_j| \le \max_{y \in Y} |y - x_j| \}.$$

Let $X \subset \mathbb{R}^2 \setminus D_j^{\max}$ and $K \subset \mathbb{C} \setminus (-\infty, 0]$ be compact sets. Then for any $(x, k) \in X \times K$ we have the following bounds for the monopole and dipole truncation errors

$$R_{j,M}(x;k) \le C_1 \left(-\ln(1-a_x) - \sum_{m=1}^M \frac{a_x^m}{m} \right)$$

$$R'_{j,M}(x;k) \le C_2 \frac{a_x^{M+1}}{1-a_x},$$
(2.7)

and

where C1 and C2 may depend on X, Y, K and

$$a_x := \frac{\max_{y \in Y} |y - x_j|}{|x - x_j|}.$$
(2.8)

To prove theorem 2.1, we need the following asymptotic formulae for Bessel functions that are uniform on the order and are valid on appropriate compact sets of $\mathbb C$ excluding the negative real axis $(-\infty,0]$. This is because we use the power series definitions for Bessel functions in ([11], §10.8) and the power series expansion for $H_n^{(1)}(z)$ is not valid for $z \in (-\infty,0]$ (as the expansion contains the term $(2i/\pi) \ln(z/2) J_n(z)$, which has a discontinuity for such z). Theorem 2.1 can be reformulated by excluding from the complex plane a different half-line than $(-\infty,0]$. This would require using a non-principal branch of the square root (to define k), of the natural logarithm ln and of Bessel functions. Also theorem 2.1 holds even if v(y) is an arbitrary unit vector (not necessarily the normal to the boundary at y).

Lemma 2.2. Let K_1 be a compact set of \mathbb{C} , K_2 be a compact set of $\mathbb{C} \setminus (-\infty, 0]$ and $n \in \mathbb{N}$. Then there exists constant C_{K_1} , \tilde{C}_{K_1} and \tilde{C}_{K_2} (independent of n) such that:

$$\left| J_n(z) - \frac{1}{n!} \left(\frac{z}{2} \right)^n \right| \le \frac{C_{K_1}}{(n+1)!} \left(\frac{|z|}{2} \right)^{n+2}, \quad \forall z \in K_1, \ n \ge 0,$$
 (2.9)

$$\left| J_n'(z) - \frac{1}{2(n-1)!} \left(\frac{z}{2} \right)^{n-1} \right| \le \frac{\tilde{C}_{K_1}}{n!} \left(\frac{|z|}{2} \right)^{n+1}, \ \forall z \in K_1, \ n \ge 1$$
 (2.10)

and

$$\left| H_n^{(1)}(z) + \frac{\mathrm{i}(n-1)!}{\pi} \left(\frac{2}{z} \right)^n \right| \le \tilde{C}_{K_2}(n-2)! \left(\frac{2}{|z|} \right)^{n-2}, \ \forall z \in K_2, \ n \ge 2.$$
 (2.11)

The proof of lemma 2.2 is included in appendix A. From lemma 2.2, we can deduce the following inequalities for J_n , J'_n (the derivative of J_n) and $H_n^{(1)}$ that are useful in the proof of theorem 2.1. Let K_1 be a compact set of $\mathbb C$ and K_2 be a compact set of $\mathbb C \setminus (-\infty, 0]$. Applying the inequality (2.9), we get that for all $z \in K_1$ and $n \ge 0$

$$|J_{n}(z)| \leq \left| J_{n}(z) - \frac{1}{n!} \left(\frac{z}{2} \right)^{n} \right| + \frac{1}{n!} \left(\frac{|z|}{2} \right)^{n}$$

$$\leq \frac{C_{K_{1}}}{(n+1)!} \left(\frac{|z|}{2} \right)^{n+2} + \frac{1}{n!} \left(\frac{|z|}{2} \right)^{n}$$

$$\leq \frac{B_{K_{1}}}{n!} \left(\frac{|z|}{2} \right)^{n} \text{ with } B_{K_{1}} = \max \left(1, C_{K_{1}} \max_{z \in K_{1}} \left(\frac{|z|}{2} \right)^{2} \right) > 0.$$
(2.12)

Similarly, one deduces from formula (2.10) and (2.11) that there exists two constants $\tilde{B}_{K_1} > 0$ and $\tilde{B}_{K_2} > 0$ such that:

$$\left| J_n'(z) \right| \le \frac{\tilde{B}_{K_1}}{(n-1)!} \left(\frac{|z|}{2} \right)^{n-1}, \quad \forall z \in K_1, \ n \ge 1$$
 (2.13)

and

$$\left| H_n^{(1)}(z) \right| \le \tilde{B}_{K_2}(n-1)! \left(\frac{2}{|z|} \right)^n, \quad \forall z \in K_2, \ n \ge 2.$$
 (2.14)

We remark that lemma 2.2 shows that inequalities (2.12)–(2.14) are optimal in the sense that they bound the functions by their leading order term. We are now ready to prove theorem 2.1.

Proof. Step 1: inequality on the monopole truncation error $R_{i,M}$.

We want to apply the lemma 2.2 to bound the terms $J_m(k|y-x_j|)$ and $H_m^{(1)}(k|x-x_j|)$ for $m \ge M+1$ appearing in the expression of $R_{j,M} = |G(x-y;k)-G_M(x-y;k)|$. Noting first that $H_{-m}^{(1)} = (-1)^m H_m^{(1)}$ and $J_{-m} = (-1)^m J_m$, we obtain that:

$$R_{j,M}(x;k) \leq \sum_{|m|>M+1} |H_m^{(1)}(k|x-x_j|)J_m(k|y-x_j|)| = \sum_{m=M+1}^{\infty} 2|H_m^{(1)}(k|x-x_j|)J_m(k|y-x_j|)|.$$

Thus, applying inequalities (2.12) and (2.13) gives that there exists $C_1 > 0$ (depending on the compacts X and K but not on the truncation index M) such that

$$R_{j,M}(x;k) \le C_1 \sum_{m=M+1}^{\infty} \frac{1}{m} a_x^m = C_1 \left(-\ln(1-a_x) - \sum_{m=1}^M \frac{a_x^m}{m} \right)$$

Step 2: inequality on the dipole truncation error $R'_{i,M}$.

For $R'_{i,M}(x;k)$, we have the following (note that θ and n depend on y)

$$\begin{split} R'_{j,M}(x;k) &= \left| \sum_{|m| \geq M+1} H_m^{(1)}(k|x-x_j|) \frac{\partial}{\partial \nu(y)} \big[J_m(k|y-x_j|) \exp[\mathrm{i} m\theta] \big] \right| \\ &= \left| \sum_{|m| \geq M+1} H_m^{(1)}(k|x-x_j|) \exp[\mathrm{i} m\theta] k \frac{(y-x_j) \cdot \nu(y)}{|y-x_j|^3} J'_m(k|y-x_j|) \right. \\ &+ H_m^{(1)}(k|x-x_j|) \exp[\mathrm{i} m\theta] J_m(k|y-x_j|) (-\mathrm{i} m) \frac{\partial}{\partial \nu(y)} \arg(y-x_j) \left| \right. \\ &\leq \sum_{|m| \geq M+1} \left| H_m^{(1)}(k|x-x_j|) k \frac{(y-x_j) \cdot \nu(y)}{|y-x_j|} J'_m(k|y-x_j|) \right| \\ &+ \left| H_m^{(1)}(k|x-x_j|) J_m(k|y-x_j|) m \frac{\partial}{\partial \nu(y)} \arg(y-x_j) \right|. \end{split}$$

Since $H_{-m}^{(1)} = (-1)^m H_m^{(1)}$ and $J_{-m} = (-1)^m J_m$ we can reduce the sum to

$$R'_{j,M}(x;k) \leq 2 \sum_{m=M+1}^{\infty} \left| H_m^{(1)}(k|x-x_j|) k \frac{(y-x_j) \cdot \nu(y)}{|y-x_j|} J'_m(k|y-x_j|) \right|$$

$$+ 2 \sum_{m=M+1}^{\infty} \left| H_m^{(1)}(k|x-x_j|) J_m(k|y-x_j|) m \frac{\partial}{\partial \nu(y)} \arg(y-x_j) \right|.$$
 (2.15)

We deal with the two latter sums separately. We start with the second sum due to its similarity to the monopole error. Noting that

$$\left| \frac{\partial}{\partial \nu(y)} \arg(y - x_j) \right| = \left| \frac{(y - x_j)_{\perp}}{|y - x_j|^2} \cdot \nu(y) \right| \le \frac{1}{|y - x_j|} \le C \tag{2.16}$$

Figure 3. The monopole (a) and dipole (b) errors (logarithmic scale), $R_{j,M}$ and $R'_{j,M}$ in (2.6) respectively, and the bounds from theorem 2.1 for a single point in space that was relatively close to the source. The colour represents the set for k as given in figure 4. For the dipoles, we cannot differentiate the different bounds as they all lie on top of each other. We observe that the dipole errors and bounds are larger. This is in line with theorem 2.1: the dipole error bound decays slower than the monopole error bound. Although some curves cannot be distinguished, the bounds always overestimate the actual errors. (Online version in colour.)

where for a vector $u = (u_1, u_2) \in \mathbb{R}^2$, $u_{\perp} = (-u_2, u_1)$ and the positive constant C is defined by $C = \max_{y \in Y} |y - x_i|^{-1}$. Thus, combining (2.12), (2.14) and (2.16) gives that

$$\sum_{m=M+1}^{\infty} m \left| H_m^{(1)}(k|x-x_j|) J_m(k|y-x_j|) \frac{\partial}{\partial \nu(y)} \arg(y-x_j) \right| \le C_3 \sum_{m=M+1}^{\infty} a_x^m, \tag{2.17}$$

where the positive constant C_3 depends only on Y, X and K.

Now, we estimate the first sum of (2.15). By virtue of the estimates (2.13) and (2.14), one gets that there exists a constant $C_4 > 0$ such that

$$\sum_{m=M+1}^{\infty} \left| H_m^{(1)}(k|x-x_j|) k \frac{(y-x_j) \cdot \nu(y)}{|y-x_j|} J_m'(k|y-x_j|) \right| \leq \frac{C_4}{|x-x_j|} \sum_{m=M+1}^{\infty} a_x^m.$$

Setting $C_5 = C_4 \max_{x \in X} |x - x_j|^{-1} > 0$, one obtains

Downloaded from https://royalsocietypublishing.org/ on 03 August 2023 by Fernando Vasquez

$$\sum_{m=M+1}^{\infty} \left| H_m^{(1)}(k|x-x_j|) k \frac{(y-x_j) \cdot \nu(y)}{|y-x_j|} J_m'(k|y-x_j|) \right| \le C_5 \sum_{m=M+1}^{\infty} a_x^m. \tag{2.18}$$

Combining (2.15), (2.17) and (2.18) yields the second inequality of (2.7).

(b) Numerical experiments for truncation error estimates

We illustrate our bounds numerically in the case where there is only one source to move, i.e. $Y = \{y\}$ and using $v(y) = (y - x_j)/|y - x_j|$. The bounds in theorem 2.1 involve a quantity a_x that can be estimated from the relative positions of x, y and x_j (respectively, the evaluation point and the original and new source positions). The bounds also involve constants C_1 , C_2 that may depend in non-obvious ways on the different choices of compact sets in space and wavenumber. To estimate C_1 (resp. C_2) for a particular choice of $(x,k) \in X \times K$, we assume the truncation error has the form predicted by the respective upper bound in (2.7), and we find the C_1 (resp. C_2) that matches the actual error explicitly for one small value of M. We repeat this estimate on a grid for $X \times K$ and then take the maxima of the estimates for C_1 (resp. C_2) over the grid.

'oyalsocietypublishing.org/journal/rsta

Phil. Trans. R. Soc. A 380: 20220073

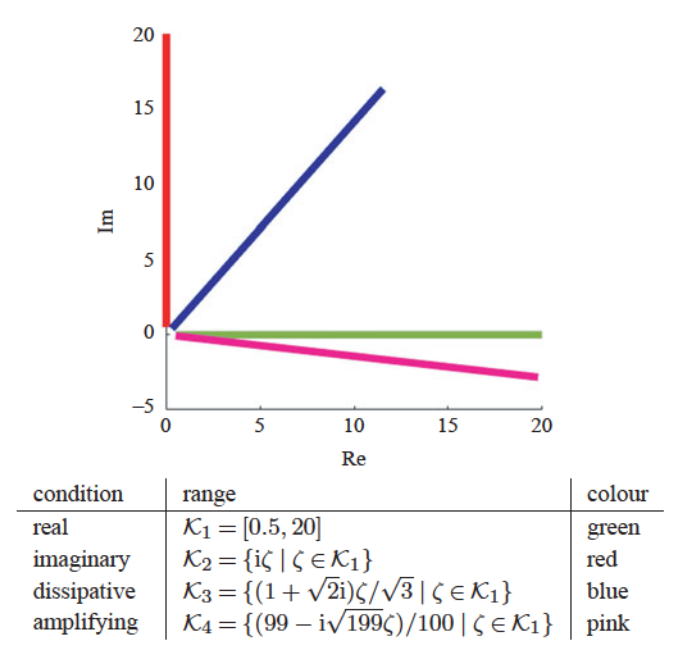


Figure 4. Wavenumber ranges used in the numerical experiments and their visualization in the complex plane. (Online version in colour.)

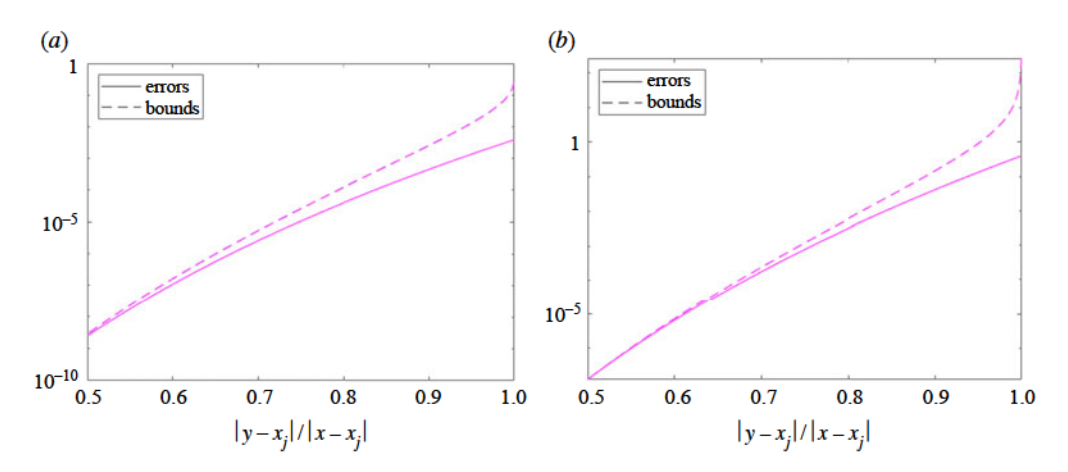


Figure 5. The monopole (a) and dipole (b) errors (logarithmic scale), $R_{i,M}$ and $R'_{i,M}$ in (2.6), respectively, and bounds for a range of points in space at a real k=1, pure imaginary k=i, complex (dissipative) $k=1/\sqrt{3}+i\sqrt{2}/\sqrt{3}$, and complex (gain) $k = (99 - i\sqrt{199})/100$ wavenumbers with the colours represented in figure 4. The plots for different wavenumbers cannot be differentiated. (Online version in colour.)

In figure 3, we show these bounds for $\{x\} \times K$, for different choices of wavenumber sets in complex plane and for the fixed evaluation point x = (0, 0.43). The original source location is y =(0,0) and it is moved to the new location $x_i = (0,0.2)$. We took M = 4 to approximate the constants C_1 and C_2 over $\{x\} \times K$ and then use our estimated C_1 and C_2 to predict the truncations errors with M = 20 terms. The different wavenumber ranges in the complex plane that we considered are summarized in figure 4. Then in figure 5, we estimated the constants C_1 and C_2 on $X \times \{k\}$ for four different wavenumbers $k \in \mathbb{C}$. Here X is the region $X = \{x \in \mathbb{R}^2 | 1/2 \le |y - x_i|/|x - x_i| \le |x - x_i| \le |x - x_i| \le |x - x_i| \le |x - x_i|$ 0.995} $\cap \{x_1 = 0\}$, i.e. the annulus for which the ratio in the geometric series ansatz belongs to [1/2, 0.995].

3. Active exterior cloaking at fixed frequency

One can achieve active cloaking by observing [5] that a distribution of monopoles and dipoles on the boundary $\partial \Omega$ of a bounded open $\Omega \subset \mathbb{R}^2$ can create a field u_c that cancels out the incident or probing field u_i inside a region Ω , while vanishing outside, or in other words satisfying (1.2). By applying the Green identities (e.g. [4]) or potential theory (e.g. [3]) the function $u_c = -u_i$ is given for $x \notin \partial \Omega$ by

$$u_c(x;k) = \int_{\partial \Omega} dS(y) \left[\frac{-\partial u_i}{\partial \nu(y)} (y;k) G(x-y;k) + u_i(y;k) \frac{\partial G}{\partial \nu(y)} (x-y;k) \right], \tag{3.1}$$

where G(x; k) is the Green function (2.1).

Downloaded from https://royalsocietypublishing.org/ on 03 August 2023 by Fernando Vasquez

Remark 3.1. The representation formula (3.1) is valid for example when Ω has Lipschitz boundary $\partial \Omega$. To see this, we assume $\overline{\Omega} \subset \mathcal{O}$, where \mathcal{O} is an open set and the incident field $u_i \in H^1_{loc}(\mathcal{O})$ solves (in the distributional sense) the Helmholtz equation $\Delta u_i + k^2 u_i = 0$ in \mathcal{O} for $k \in \mathbb{C} \setminus \{0\}$. Then as $-\Delta u_i = k^2 u_i$ on \mathcal{O} , one easily proves by interior elliptic regularity of the minus Laplacian operator (applying iteratively theorem 2, p. 314 of [20]) that $u_i \in C^{\infty}(\overline{\Omega})$.

We point out that $u_c = -u_i \in C^{\infty}(\overline{\Omega})$ and the outward normal vector $v(y) \in L^{\infty}(\partial \Omega)$ since $\partial \Omega$ is a Lipschitz boundary. Thus, it is clear that the Dirichlet trace u_i is smooth on $\partial \Omega$ and that the Neumann trace $[\partial u_i/\partial v(y)](y;k)$ is in $L^{\infty}(\partial \Omega)$. Hence, the integrand in (3.1) is integrable as a sum of two products of $L^{\infty}(\partial \Omega)$ functions. Indeed since we have $x \notin \partial \Omega$, the Green function G(x-y;k) is smooth for $y \in \partial \Omega$ and its normal derivative $[\partial G/\partial v(y)](x-y;k)$ is in $L^{\infty}(\partial \Omega)$ as a function of y.

To get *exterior* cloaking, the idea is to move the monopoles and dipoles on the portions $\partial \Omega_j$ of the boundary $\partial \Omega$ to the new source locations x_j . Formally, this can be done by replacing the Green function and its normal derivative in the representation formula (3.1) by their series expansions (2.2) and (2.4). Theorem 3.2 and remark 3.1 allow to permute the order of the series and the integral over $\partial \Omega$ (since the series is normally convergent with respect to y). Thus we can express the new cloaking field as

$$u_{e}(x;k) = \sum_{j=1}^{N_{\text{dev}}} \sum_{m=-\infty}^{\infty} b_{j,m} V_{m}(x - x_{j};k),$$
(3.2)

where V_m are multipolar sources (2.3) and the coefficients $b_{j,m}$ are given by (3.4) in terms of integrals over the $\partial \Omega_j$, identical to those obtained in [2]. We emphasize that theorem 3.2 is valid for complex k with the exception of the negative real axis, whereas the result in [2] is only proven for real k positive. Moreover, theorem 3.2 leverages on the Graf addition formula truncation error estimates in theorem 2.1, to give the truncation error when we consider instead the truncated fields:

$$u_e^{(M)}(x;k) = \sum_{j=1}^{N_{\text{dev}}} \sum_{m=-M}^{M} b_{j,m} V_m(x - x_j; k).$$
(3.3)

This error estimate is novel and applies to the results in [2].

Theorem 3.2. Let $\Omega \subset \mathbb{R}^2$ be a bounded open set with Lipschitz boundary $\partial \Omega$. Assume u_i is a $H^1_{loc}(\mathcal{O})$ solution to the Helmholtz equation, where \mathcal{O} is an open set containing $\overline{\Omega}$. Define the region $R = R_1 \cup \cdots \cup R_{N_{dev}}$, i.e. the union of the discs R_j in (1.4). Let K be a compact subset of $\mathbb{C} \setminus (-\infty, 0]$ and X a compact subset of $\mathbb{R}^2 \setminus R$. Define the coefficients $b_{j,m}$ in (3.2) and (3.3) by

$$b_{j,m} = \int_{\partial \Omega_j} dS(y) \left[-\frac{\partial u_i}{\partial \nu(y)} (y;k) U_m(y - x_j;k) + u_i(y;k) \frac{\partial U_m(y - x_j;k)}{\partial \nu(y)} \right], \tag{3.4}$$

where $j = 1, ..., N_{dev}$, $m \in \mathbb{Z}$ and $U_m(x;k) = J_m(k|x|) \exp[-i marg(x)]$. Then there exists a constant C > 0 (which may depend on K, X, u_i and $\partial u_i/\partial v(y)$) such that for any $(x,k) \in X \times K$,

$$|u_c(x;k) - u_e^{(M)}(x;k)| \le C \frac{a^{M+1}}{1-a},$$
 (3.5)

$$a = \max_{x \in X} \max_{j=1,\dots,N_{\text{dev}}} \max_{y \in \partial \Omega_j} \frac{|y-x_j|}{|x-x_j|} < 1.$$

In particular for any $x \notin R$ and $k \notin (-\infty, 0]$, we have $u_c(x; k) = u_e(x; k)$.

Remark 3.3. The integral appearing in the definition of the $b_{j,m}$ in (3.4) can be expressed as a series when the incident field u_i is given in terms of its cylindrical wave expansion ([36], Theorem 2). Although the series expansion is proven for the two-dimensional Helmholtz equation with k > 0, we conjecture it is valid for complex k.

Remark 3.4. Controlling fields outside of a bounded open set Ω can be useful for the mimicking problem (making a scatterer inside Ω look like another one) or for cloaking a source inside Ω . This requires an *exterior* version of the Green representation formula (3.1), which is valid for $\text{Im}(k) \geq 0$, when the field to reproduce u_i is a solution to the Helmholtz equation outside of Ω and satisfies the Sommerfeld radiation condition (e.g. [37], Theorem 3.3). We are not aware of the validity of this result for gain media (Im(k) < 0). Therefore, we anticipate that theorem 3.2 can be adapted to control fields outside of R for $\text{Im}(k) \geq 0$ and $k \notin (-\infty, 0]$.

(a) Proof of theorem 3.2

Proof. We rewrite the boundary integral representation (3.1) of the cloaking field u_c as a sum of integrals over the portions $\partial \Omega_i$ of the boundary. We then apply (2.2) to yield

$$u_{c}(x) = \sum_{j=1}^{N_{\text{dev}}} \int_{\partial \Omega_{j}} dS(y) \left[\frac{-\partial u_{i}}{\partial \nu(y)} (y) \frac{i}{4} \sum_{m=-\infty}^{\infty} V_{m}(x - x_{j}) U_{m}(y - x_{j}) + u_{i}(y) \frac{i}{4} \frac{\partial}{\partial \nu(y)} \sum_{m=-\infty}^{\infty} V_{m}(x - x_{j}) U_{m}(y - x_{j}) \right],$$

$$(3.6)$$

which holds for $x \notin R$. We approximate the cloak field by $u_e^{(M)}$ with coefficients $b_{j,m}$ chosen as in (3.4) to match the $|m| \le M$ terms in the series in (3.6). Thus the error we make by approximating $u_c(x)$ by $u_e^{(M)}$ at some $x \notin R$ can be bounded by

$$\begin{aligned} |u_c(x) - u_e^{(M)}(x)| &= \left| \sum_{j=1}^{N_{\text{dev}}} \int_{\partial \Omega_j} dS(y) \left[\frac{-\partial u_i}{\partial \nu(y)}(y) \frac{i}{4} \sum_{|m| \ge M+1} V_m(x - x_j) U_m(y - x_j) \right. \\ &+ u_i(y) \frac{i}{4} \frac{\partial}{\partial \nu(y)} \sum_{|m| \ge M+1} V_m(x - x_j) U_m(y - x_j) \right] \\ &\leq \sum_{j=1}^{N_{\text{dev}}} \int_{\partial \Omega_j} dS(y) \left[\left| \frac{-\partial u_i}{\partial \nu(y)}(y) \frac{i}{4} \right| \left| \sum_{|m| \ge M+1} V_m(x - x_j) U_m(y - x_j) \right| \right. \\ &+ \left| u_i(y) \frac{i}{4} \right| \left| \frac{\partial}{\partial \nu(y)} \sum_{|m| \ge M+1} V_m(x - x_j) U_m(y - x_j) \right| \right]. \end{aligned}$$

We notice that

$$R_{j,M}(x;k) = \left| \sum_{|m| \ge M+1} V_m(x-x_j) U_m(y-x_j) \right|$$

and

$$R'_{j,M}(x;k) = \left| \frac{\partial}{\partial \nu(y)} \sum_{|m| \ge M+1} V_m(x - x_j) U_m(y - x_j) \right|,$$

allowing us to apply theorem 2.1 to bound the truncation by remainders of a geometric series. It follows that there exists two positive constants $C_{1,j}$ and $C_{2,j}$ that depend on the compact sets X, $Y_j = \partial \Omega_j$ and K such that

$$|u_c(x) - u_e^{(M)}(x)| \leq \sum_{j=1}^{N_{\text{dev}}} \int_{\partial \Omega_j} dS(y) \left(\left| \frac{\partial u_i}{\partial \nu(y)}(y) \frac{1}{4} C_{1,j} \right| + \left| u_i(y) \frac{1}{4} C_{2,j} \right| \right) \frac{a_{x,j}^{M+1}}{1 - a_{x,j}},$$

with

$$a_{x,j} = \frac{\max_{y \in \partial_{\Omega_j}} |y - x_j|}{|x - x_j|}.$$

Setting $C_1 = \max_{j=1,\dots,N_{\text{dev}}} C_{1,j}$ and $C_2 = \max_{j=1,\dots,N_{\text{dev}}} C_{2,j}$, it follows that

$$|u_c(x) - u_e^{(M)}(x)| \le n \max_j |\partial \Omega_j| \tilde{C} \frac{a^{M+1}}{1 - a}, \tag{3.7}$$

where, using that $u_i \in C^0(\partial \Omega)$ and $\partial u_i/\partial v(y)$ is $L^{\infty}(\partial \Omega)$ by remark 3.1, we introduced

$$\tilde{C} = \operatorname{ess\,sup}_{y \in \partial \Omega} \left| \frac{\partial u_i}{\partial \nu(y)}(y) \frac{1}{4} C_1 \right| + \max_{y \in \partial \Omega} \left| u_i(y) \frac{1}{4} C_2 \right| \tag{3.8}$$

and

Downloaded from https://royalsocietypublishing.org/ on 03 August 2023 by Fernando Vasquez

$$a = \max_{x \in X} \max_{j=1,\dots,n} a_{x,j} < 1. \tag{3.9}$$

The error bound (3.5) follows by letting $C = N_{\text{dev}} \tilde{C} \max_j |\partial \Omega_j|$. In addition, we have for $x \notin R$ and $k \in \mathbb{C} \setminus (\infty, 0]$ that $|u_c(x) - u_e(x)| = \lim_{M \to \infty} |u_c(x) - u_e^{(M)}(x)| = 0$ since a < 1. Hence we have $u_c = u_e$ for $x \notin R$. The fields do not agree for $x \in R$, because for at least one $j \in \{1, \ldots, N_{\text{dev}}\}$, the series in (3.2) diverges.

(b) Stability through the maximum principle

Helmholtz equation solutions satisfy a strong maximum principle if $Re(k^2) < 0$ or equivalently

$$|\operatorname{Im}(k)| > |\operatorname{Re}(k)|. \tag{3.10}$$

Although we use this result for constant isotropic media, it has been proved in the very general context of the Helmholtz equation with anisotropic heterogeneous media ([26], corollary 2.1). Another proof in the case of isotropic heterogeneous media appears in ([27], theorem 6).

We now state the strong maximum principle. By interior regularity (see remark 3.1), a solution $u \in H^1_{loc}(\mathcal{O})$ to the Helmholtz equation in an open set \mathcal{O} with a wavenumber k satisfying (3.10), is $C^{\infty}(\overline{B})$ on any open bounded subset \mathcal{B} with Lipschitz boundary ∂B satisfying $\overline{\mathcal{B}} \subset \mathcal{O}$. Thus, one can apply the strong maximum principle on the set \mathcal{B} to get on one hand that

$$\max_{x \in \overline{\mathcal{B}}} |u(x)| = \max_{x \in \partial \mathcal{B}} |u(x)|,$$

and on the other hand that the maximum of |u| is only reached on the boundary $\partial \mathcal{B}$ of \mathcal{B} . We note that the *strong* maximum principle is not valid for k outside the region (3.10) as one can find examples of solutions violating it [26].

In particular if u and v are smooth solutions to the Helmholtz equation in \mathcal{B} with k satisfying (3.10), the maximum of the error |u(x)-v(x)| is attained *only* at the boundary $\partial \mathcal{B}$. In other words, the error within the domain is controlled by the error on the boundary (the Dirichlet data). This can be viewed as a form of stability for the boundary integral representation (3.1). Moreover, u_e and $u_e^{(M)}$ are $C^{\infty}(\overline{\mathcal{B}})$ solutions to the Helmholtz equation on \mathcal{B} , where \mathcal{B} is a bounded open set such that $\overline{\mathcal{B}} \subset \mathbb{R}^2 \setminus R$ (see theorem 3.2). Therefore, we can conclude from the maximum principle that the truncation error of exterior cloaking $(|u_e(x)-u_e^{(M)}(x)|)$ reaches its maximum over $\overline{\mathcal{B}}$ only on the boundary $\partial \mathcal{B}$. Finally, we point out that when numerically evaluating the boundary representation formula (3.1), we use finitely many monopole and dipole sources on the domain

Figure 6. (a) The configuration of the exterior cloak used for four exterior sources (x_j) to maximize the region where an object can be dissimulated (the blue striped region), we take $\delta_D = \sqrt{2}\delta_C$. (b) Cloaking region with smallest inscribed circle with radius r_{ζ_0} and largest circumscribed circle with radius r_{ζ_0} . (a) Inner and exterior cloak configuration, (b) cloak with in/circumscribed circles. (Online version in colour.)

 $\partial\Omega$. Following the same argument, the error we make with this discretization is also maximum on the boundary of any bounded domain \mathcal{B} such that $\overline{\mathcal{B}} \subset \mathbb{R}^2 \setminus \partial\Omega$. We numerically illustrate in figure 9 that the maximum principle predicts that the maximum cloaking errors occur on the boundary of a region and not inside.

(c) Numerical experiments

Downloaded from https://royalsocietypublishing.org/ on 03 August 2023 by Fernando Vasquez

We explain how we evaluate the truncated cloak field $u_e^{(M)}$ in §3c(i). Then the truncation errors are predicted in §3c(ii) using the error bounds in theorem 3.2. Finally, we explain in §3c(iii) how we calculate scattered fields when $\text{Im}(k) \ge 0$.

(i) Evaluation of the cloak field

We illustrate theorem 3.2 numerically using a disc region Ω and n=4 sources, as shown in figure 6. While we chose to illustrate exterior cloaking with four multipolar sources, only three are necessary in two dimensions to give a non-empty region cloaking [6]. Cloaking fields $u_e^{(M)}$ with M=22 are shown in figure 7 for several representative wavenumbers on the square $[0,10]^2$ using a 200×200 uniform grid. The disc Ω is centred at (5,5) and with radius $\delta_C=10/6$. The x_j are uniformly spaced on a circle of same centre and radius δ_D (figure 6), where δ_D is chosen to maximize the area of the cloaking region for δ_C fixed. The optimization is done via a simple geometric argument similar to [6] and gives $\delta_D=5\sqrt{2}/3$. The incident field is generated by a point source at y=(2,5). To evaluate the truncated exterior cloaking field, $u_e^{(M)}$, we use an equispaced discretization of $\partial\Omega$, into points y_i with $i=1,\ldots,n_{int}$. We split $\partial\Omega$ into n=4 regions each associated with a new source location x_j . We choose n_{int} so that there is an equal number of discretization points of $\partial\Omega$ for each $\partial\Omega_j$ and choose the x_j such that $\max_{y_i\in\partial\Omega_j}|y_i-x_j|$ is equal for all j in order to keep the size of the theoretical divergence regions R_j of our devices equal. The integrals over $\partial\Omega_j$ that determine the coefficients $b_{j,m}$ in theorem 3.2 are approximated using the midpoint rule (so that the total integral over $\partial\Omega$ is the trapezoidal rule).

We note that the colour scale in figure 7 is deliberately limited to exclude the large fields near the new source locations x_i which are due to the singularity of $u_e^{(M)}$ at the x_i . This may seem to be

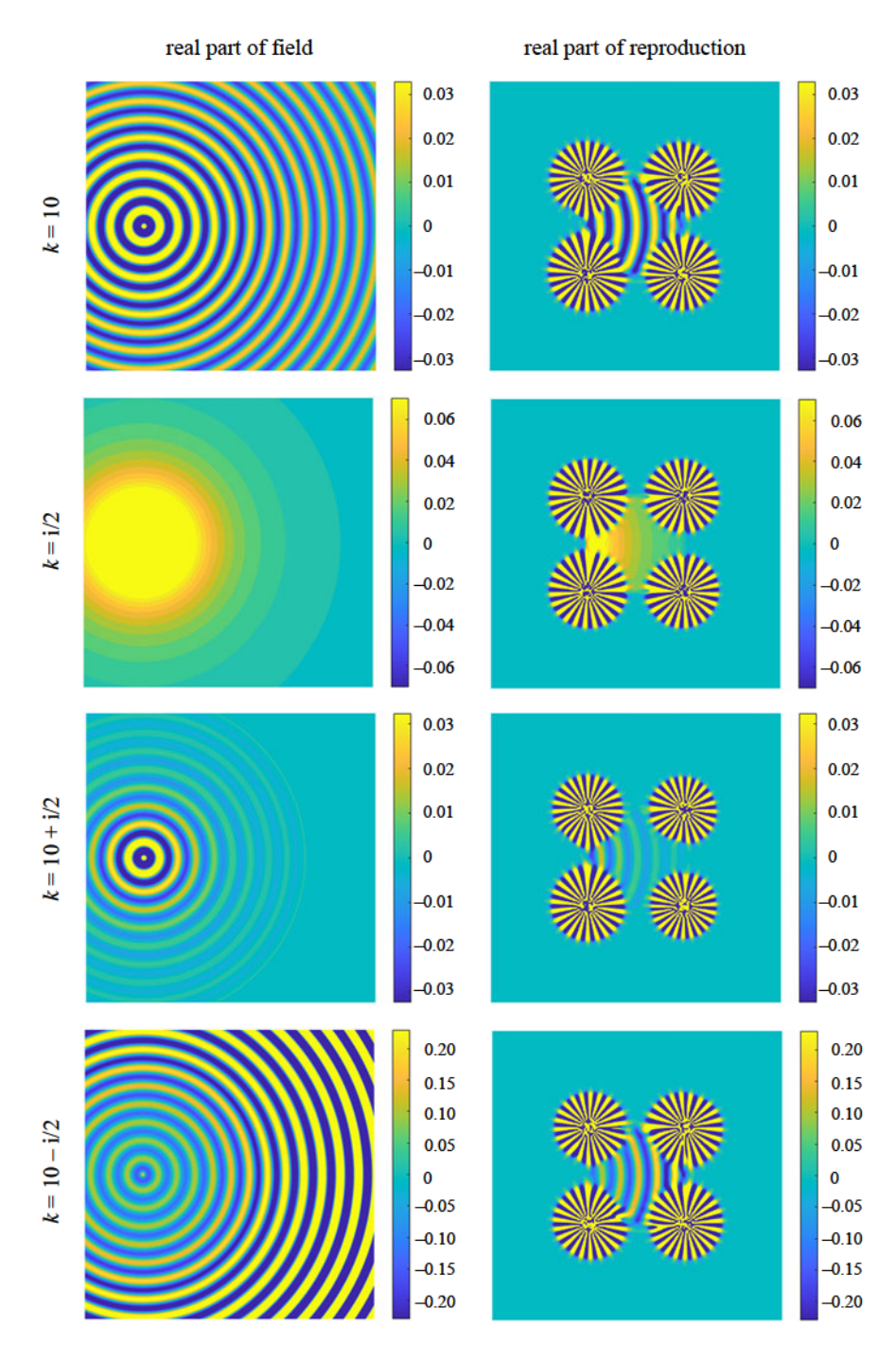


Figure 7. Field reproductions (b) and the original field (a) at different wavenumbers on the square $[0, 10]^2$ with a point source located at (2, 5). The colour scale was kept the same for each k and was chosen to highlight the different behaviours of the point sources for different k. (Online version in colour.)

an impediment to physically realize such cloaking devices. However, as noted in [6], it is possible to use the Green exterior representation formula (valid for $Im(k) \ge 0$, see [37], Theorem 3.3) to replace the multipolar sources by a distribution of monopoles and dipoles on some boundary enclosing each of the x_j . Since the cloak field $u_e^{(M)}$ is smaller, we expect it is easier to realize in practice. The drawback is that these 'extended cloaking devices' leave only small gaps between

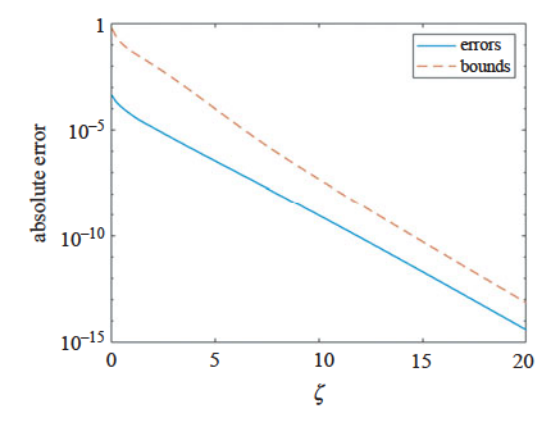


Figure 8. Predicted and actual maximum error (logarithmic scale) on circles of radius slightly larger than r_{c_0} and smaller than r_{c_0} , which are outside of the divergence region of the cloak field. The abscissa corresponds to the parameter ζ for the segment of wavenumbers \mathcal{K}_3 , as defined in figure 4. (Online version in colour.)

the cloaked region and the exterior. By theorem 3.2, we expect that $|u_e^{(M)}(x)| \to \infty$, when $M \to \infty$ for $x \in R$. So increasing M leads to smaller gaps; there is a trade-off between getting larger gaps and truncating the ideal cloak field u_e , see (3.2).

(ii) Computation of error bounds and the maximum principle

In order to use the error bounds from theorem 3.2 in our particular geometric set-up, we define the radius r_{C_i} (resp. r_{C_O}) of the largest (resp. smallest) inscribed (resp. circumscribed) circle that is inside (resp. outside) the divergence region R (defined in theorem 3.2). The inscribing and circumscribing circles are represented in figure 6. We recall from (3.7) that the cloak field truncation error can be bounded by the truncation error of a geometric series with ratio a that is determined by the relative positions of the $\partial \Omega_i$, the x_i and the region of interest where we want to evaluate the fields, see (3.9). Since we expect the cloaking fields to diverge close to R, it does not make sense to evaluate the errors on the inscribing and circumscribing circles. We do it instead on slightly smaller or larger circles of radii $r_{C_0} + 0.1\delta_C$ and $r_{C_i} - 0.1\delta_C$. If we take the region X from theorem 3.2 to be the union of these two circles and symmetric x_i , a simple geometric argument yields that there are eight points in X that attain the maximum over X in the definition of a (3.9). At each of these points, the ratio of the geometric series ansatz is the same, so we can conclude the truncation error can be bounded by $C(1-a^{M+1})/(1-a)$, where a < 1, but the constants C depend on the point. We first estimate the constant C at a point x by using the 'empirical method' we used in §2b. In other words, we find the C for which $|u_e^{(3)}(x) - u_e(x)|$ is equal to $C(1 - a^{M+1})/(1 - a)$ with M = 3. Then we take the worst case scenario, i.e. the largest of such C for the eight points in X that we considered. We emphasize that this is a heuristic meant to simplify the exhaustive method, where we would have to evaluate the largest C for all $x \in X$. We summarize in figure 8 the application of this heuristic for wavenumbers $k \in \mathcal{K}_3$ (as defined in figure 4). In these experiments, we used 128 equispaced discretization points for $\partial \Omega$, $\delta_C = 10/6$ and $\delta_D = 5\sqrt{2}/3$. Finally the incident field we used for this experiment was a point source located at x = (8,5). As can be seen from figure 8, the error bound we obtain for M = 22 overestimates the actual error and follows the same trend for varying wavenumber.

We illustrate in figure 9 that when |Im(k)| > |Re(k)|, the maximum principle (§3b) can be used to predict where the maximum cloaking error occurs. In fact the wavenumbers we used for figure 8 also allow us to use the maximum principle to observe that a bound for the truncation error on the boundary of the circle with radius $r_{C_i} - 0.1\delta_C$ automatically leads to a bound on the whole disc of same radius.

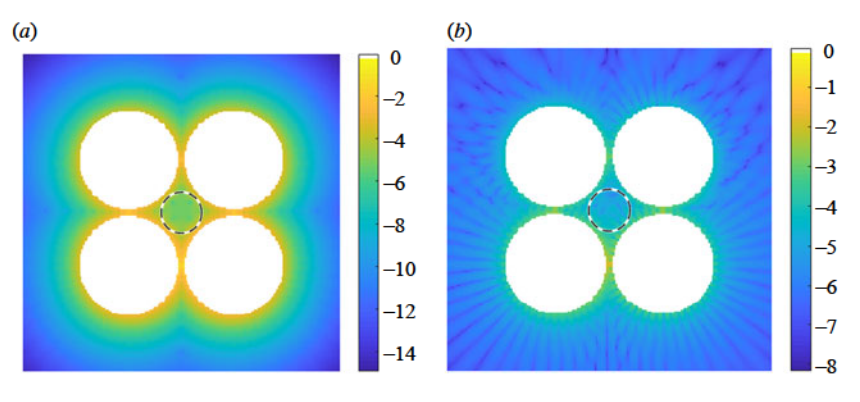


Figure 9. We display the cloaking field truncation error $\log_{10} |u_e^M - u_e|$ (outside of the 'extended cloaking devices' in white) corresponding to (a) k = i/2 and (b) k = 10 + i/2. We note that (a) (resp. (b)) corresponds to the second (resp. third) row in figure 7. By applying the maximum principle on the disc \mathcal{B} (dashed curve), we see that the maximum error is attained on $\partial \mathcal{B}$ in (a) but not in (b). The difference is that the wavenumber in (a) satisfies |Im(k)| > |Re(k)| so a version of the maximum principle applies, see also figure 2. (Online version in colour.)

(iii) Calculating scattered fields for $\text{Im}(k) \geq 0$

To demonstrate cloaking, we recall how to calculate scattered fields from a sound-soft (or homogeneous Dirichlet) obstacle A. Here we follow the discussion in [4]. We assume for simplicity that the obstacle A is a bounded domain with C^2 boundary ∂A (for similar results in the more general case of Lipschitz boundary see [38], §9). The scattering problem can be posed as the following exterior Dirichlet problem

$$\Delta u_s + k^2 u_s = 0$$
, $x \in \mathbb{R}^2 \setminus A$

and

Downloaded from https://royalsocietypublishing.org/ on 03 August 2023 by Fernando Vasquez

$$u_s = -u_i, \quad x \in \partial A,$$

where u_s also satisfies the Sommerfeld radiation condition

$$\lim_{|x|\to\infty}|x|^{1/2}\left(\frac{\partial}{\partial|x|}-\mathrm{i}k\right)u_s(x)=0,$$

where $\partial/\partial|x|$ denotes the radial derivative and the limit is uniform for all directions x/|x| (see [4], §3.4). The exterior Dirichlet problem has a unique solution $u_s \in H^1_{loc}(\mathbb{R}^2 \setminus A)$ for $Im(k) \geq 0$ and $u_i|_{\partial\Omega} \in H^{1/2}(\partial A)$, e.g. ([4], §3.2). This is clearly the case under the assumptions in remark 3.1, since $u_i \in C^{\infty}(\partial\Omega)$.

We seek the scattered field in the form of a mixed single and double-layer potential $\psi \in H^{1/2}(\partial A)$ satisfying

$$u_s(x;k) = \int_{\partial A} dS(y) \left(\frac{\partial G}{\partial \nu(y)} (x - y; k) - i \eta G(x - y; k) \right) \psi(y), \tag{3.11}$$

where $\eta \neq 0$, satisfying $\eta \text{Re}(k) \geq 0$, is a coupling parameter. This choice guarantees invertibility for Im(k) = 0 (e.g. [37], §3.6) but it is not necessary when Im(k) > 0. The corresponding boundary layer operators are defined for $x \in \partial A$ by

$$(S\varphi)(x) := 2 \int_{\partial A} dS(y) [G(x-y;k)\varphi(y)]$$

and

$$(K\varphi)(x) := 2 \int_{\partial A} dS(y) \left[\frac{\partial G}{\partial \nu(y)} (x - y; k) \varphi(y) \right],$$

for the single and double-layer potential, respectively. We note that the operators can be taken as bounded operators $S, K: L^2(\partial A) \to L^2(\partial A)$ (e.g. ([39], Theorem 4.4.1) for smooth ∂A or ([38], ch. 6) for C^2 or even Lipschitz ∂A). We also need the following jump relations, letting $z \in \mathbb{R}^2 \setminus \partial A$

$$\lim_{z \to x} \int_{\partial A} dS(y) [G(z - y; k)\varphi(y)] = \frac{[S\varphi](x)}{2}$$

$$\lim_{z \to x^{+}} \int_{\partial A} dS(y) \left[\frac{\partial G}{\partial \nu(y)} (z - y; k)\varphi(y) \right] = \frac{1}{2} \left(\varphi(x) + [K\varphi](x) \right),$$
(3.12)

and

where $z \to x^+$ denotes the limit from the exterior of *A*. Taking the limit of (3.11) as we approach the boundary of *A* from the exterior and applying (3.12) yields

$$\psi + K\psi - i\eta S\psi = -2u_i|_{\partial A},\tag{3.13}$$

which has a unique solution ψ (e.g. [4], §3.2). We assume that ∂A admits a 2π -periodic parametrization of the form

$$q(\tau) = (x_1(\tau), x_2(\tau)), \quad 0 \le \tau \le 2\pi,$$

that is $q([0,2\pi]) = \partial A$ and q is assumed smooth for our numerical experiments. As noted in e.g. ([4], §3.5), (3.13) is an integral equation of the second kind with a weakly singular kernel. There are several methods to discretize such integral equations, e.g. [40] for a review. Here we chose the Kapur–Rokhlin method [41], which is based on the trapezoidal rule for periodic functions. In this method, the unknowns are the values of ψ at uniformly spaced points of $[0,2\pi]$. To account for the singularity, the entries in a band of the system matrix are weighted so that the quadrature is exact for polynomials of a given order (sixth order in our case).

We do note that the Kress quadrature [4] was used in [6] for computing the scattered fields with k > 0 and is spectrally accurate. Unfortunately, accuracy of the Kress quadrature degrades for complex k. Indeed, the Kress quadrature is obtained by splitting the singular kernel into a singular and non-singular part. The latter requires the evaluation of $J_0(kr)$, which grows exponentially in Im(k) for fixed k 0, e.g. ([11], §10.7). The correction weights for the Kapur–Rohklin method only depend on the type of singularity and order of the method. Thus the Kapur–Rohklin is better adapted for complex k. Convergence for k complex follows from convergence of the method for the real and imaginary parts, considered individually.

4. Active exterior cloaking for the heat equation

We now apply the single wavenumber exterior cloaking approach to the time domain heat equation. We recall in §4a other cloaking approaches. We then use the Fourier–Laplace transform to obtain the Helmholtz equation from reasonable heat equation solutions (§4b). The exterior cloaking approach is applied for different wavenumbers and then put together again in §4c via the inverse Laplace transform. The details of the discrete Fourier transform-based algorithm we used for this purpose are given in §4d.

(a) Other cloaking approaches for the heat equation

Cloaking for the heat equation was originally introduced through a change of coordinate system [42], inspired by transformation optics [43,44]. However, this approach leads to an extreme anisotropic thermal conductivity, and even a thermal cloak designed through a regularized geometric transform suffers from limited efficiency in the transient regime [42]. A good thermal cloak efficiency requires as many as 10 000 isotropic concentric layers to finely approximate its spatially varying anisotropic conductivity [45]. Thus, fabricated metamaterial cloaks with a limited number of layers suffer from reduced efficiency in the transient regime [46–50]. For other passive cloaking and mimicking approaches see e.g. [51,52]. Recent advances in thermal cloaking are thus underpinned by inverse homogenization problems that require heavy computational resources. On the other hand, thermoelectric devices have been proposed to pump the heat flow

accurately from one side of a thermal cloak to the other side by adjusting the input current, so that the background temperature field can be restored in a stationary regime [53,54]. In our former work [55], we envisioned using Peltier devices (surrounding the object to cloak) to control transient thermal fields generated by a source. The approach we present here can be viewed as a generalization of that in [56] that considered a single dipole source placed inside the object to cloak in the stationary regime. There should be a trade-off between using a single dipole source and numerous monopole and dipole sources to achieve efficient thermal cloaking in the transient regime, which is what motivated the present work. Numerical optimization techniques can also be used to achieve active exterior cloaking for the heat equation [57]. Our analysis is performed in the frequency regime, where we can extend results of [6] to the Helmholtz equation with complex wavenumbers. Results are then translated in the time domain through the inverse Fourier–Laplace transform.

Remark 4.1. Since our approach is based on the Laplace transform of the time domain heat equation, it is more convenient to assume a zero initial condition. Indeed a non-zero initial condition would appear as a source term for the Helmholtz equation, which would prevent us from using the interior reproduction formula (3.1). However, as noted in [55], if the initial condition is a steady-state solution to the heat equation (i.e. harmonic) we can use the linearity of the heat equation to apply our approach to u(x,t) - u(x,0).

Remark 4.2. As we see next, we obtain solutions to the heat equation that achieve exterior cloaking but they can be large as we get close to the new source locations x_j . However, as noted in [55], it is conceivable to use Peltier devices to physically implement the interior/exterior reproduction formula for the time domain heat equation [58]. This procedure allows to replace point-like sources by active surfaces that we call 'extended cloaking devices', which would keep the temperatures at levels that would be practical to implement.

(b) From time domain to frequency domain

We now apply our frequency domain cloaking approach to the heat equation. The temperature u(x, t) (measured in Kelvin) in a homogeneous isotropic medium satisfies the heat equation

$$\rho c \frac{\partial \mathfrak{u}}{\partial t} = \kappa \Delta \mathfrak{u} + \mathfrak{h}, \quad \text{for } t > 0, \tag{4.1}$$

where t is the time (s), ρ is the mass density (kg m⁻²), c is the specific heat (J K⁻¹ kg⁻¹) and κ is the thermal conductivity (W K⁻¹). Here we assume that ρ , c and κ are positive constants. The source term is $\mathfrak{h}(x,t)$ (W m⁻²) and assumed causal, i.e. $\mathfrak{h}(x,t)=0$ for t<0. For simplicity, we assume a zero initial condition and consider

$$\frac{\partial \mathfrak{u}}{\partial t} = \sigma \Delta \mathfrak{u} + \frac{\mathfrak{h}}{\rho c}, \quad \text{for } t > 0, \tag{4.2}$$

where $\sigma = \kappa/\rho c$ is the thermal diffusivity $(m^2 s^{-1})$. Assuming further that the source term $\mathfrak{h} \in L^1_{\mathrm{loc}}((0,\infty),L^2(\mathbb{R}^2))$ satisfies the growth condition (1.7) with $L^2(\mathbb{R}^2)$ norm, $\alpha \geq 0$ and an integer $p \geq 0$, we can see that $e^{-\xi t}\mathfrak{h}(x,t) \in L^2([0,\infty),L^2(\mathbb{R}^2))$ for any $\xi > \alpha$. Using ([15], Corollary 2, p. 238) it is possible to conclude that (4.2) admits a unique solution $\mathfrak{u}(x,t)$ satisfying $e^{-\xi t}\mathfrak{u}(x,t) \in L^2([0,\infty),H^2(\mathbb{R}^2))$ for any $\xi > \alpha$. This allows to define the Fourier–Laplace transform (1.6) of all terms in (4.2) on the half plane \mathbb{C}^+_α , thus obtaining the Helmholtz equation

$$\Delta u(x;\omega) + \frac{\mathrm{i}\omega}{\sigma}u(x;\omega) = -\frac{h(x,\omega)}{\kappa},\tag{4.3}$$

where the wavenumber is $k = i\sqrt{-i\omega/\sigma}$, using the principal value of the square root and h is the Fourier–Laplace transform of \mathfrak{h} . We note that $\operatorname{Re}(k^2) = \operatorname{Re}(i\omega/\sigma) < 0$, whenever $\operatorname{Im}(\omega > 0)$, which guarantees that the Helmholtz equation satisfies a form of the maximum principle for any $\omega \in \mathbb{C}^+_\alpha$ (since $\alpha \geq 0$), for x outside of the support of the source h (see §3b and (1.8) for the definition of \mathbb{C}^+_α).

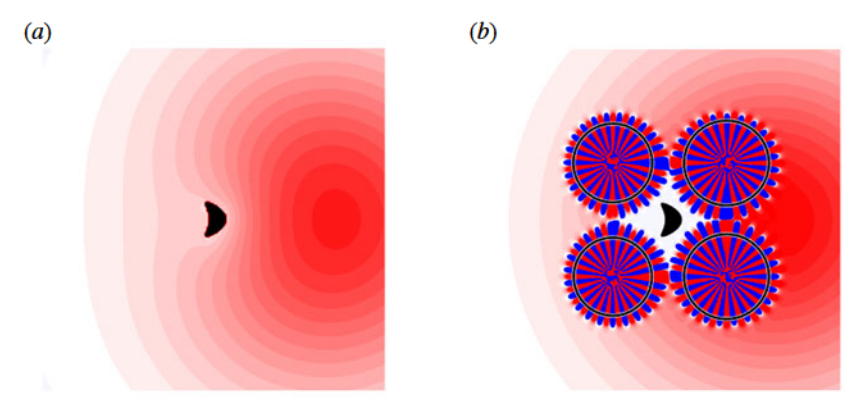


Figure 10. (a) Temperature distribution at time t=4 with $\sigma=1.5$ (see (4.2)) resulting from a point source at location (8, 5) in the presence of a 'kite' object with homogeneous Dirichlet boundary condition. (b) The same object and source as in (a), but with the cloaking devices activated. The temperatures outside of the black circles are bounded by $u_{max}\approx 6.2$ (see (4.4)) for $t\in[0,4]$. The computational domain was $[0,10]^2$. The linear colour scale spans temperatures in [-0.0133,0.0133] and ranges from blue (negative) to red (positive), with zero represented in white. (See also the movie in the electronic supplementary material.) (Online version in colour.)

(c) Numerical experiments

Downloaded from https://royalsocietypublishing.org/ on 03 August 2023 by Fernando Vasquez

We show in figure 10 a numerical simulation of active exterior cloaking of a Dirichlet object (a 'kite' with constant zero temperature at its boundary) and compare it with the case where there are no cloaking devices. For the purposes of the numerical experiments, we non-dimensionalized (4.2) choosing $\sigma = 1.5$ and $\rho = c = 1$. As can be seen from the time snapshot in figure 10, the isotherm lines without the cloaking devices are significantly different from those of the point source that we used as the incident field u_i , this is because of the field 'scattered' by the object. For an observer far from the cloaking devices, the isotherms appear consistent with those of a point source, so it is hard for the observer to detect the object from thermal measurements. In our numerical experiments, the region Ω is a disc centred at (5,5) and with radius $\delta_C = 10/6$ enclosing the 'kite' object. We moved the distribution of monopoles and dipoles to four new source locations determined as in figure 6 with $\delta_D = 5\sqrt{2}/3$. We note that three new source locations would have been sufficient, as in [6]. The fields are calculated on $[0,10]^2$ using a 200×200 uniform grid. The incident field is generated by a point source at y = (8,5). The integral in theorem 3.2 is approximated with 256 uniformly placed points and the series in (3.3) uses the truncation M = 22. The boundary of the scatterer is discretized using 512 equally spaced points on the parametric representation of ∂A and the scattered fields (in the frequency domain) are calculated according to the scheme in §3c. The frequency domain calculation is performed for 2050 frequencies and the Laplace transform is inverted using a Fast Fourier Transform-based method (see §4d).

Because the multipolar sources are singular at the x_j , the cloaking field diverges as we approach the x_j . This could limit the physical implementation (e.g. because the material starts degrading with such high temperatures). Of course, we may use the Green exterior representation formula (e.g. [55,58]) to replace each of the multipolar sources by a monopole and dipole distribution on surfaces containing the multipolar source. These active surfaces or 'extended cloaking device' could be realized in practice using Peltier devices [53] and the temperatures do not need be unreasonably large. To illustrate this, we display in figure 10 black circles centred at the new source positions, outside of which we are guaranteed to have $|\mathfrak{u}_e^{(M)}(x,t)| \leq \mathfrak{u}_{max}$. Our choice \mathfrak{u}_{max} is

$$u_{\text{max}} = 100 \max_{(x,t) \in \Omega \times [0,T]} |u_i(x,t)|.$$
 (4.4)

Phil. Trans. R. Soc. A 380: 2022007:

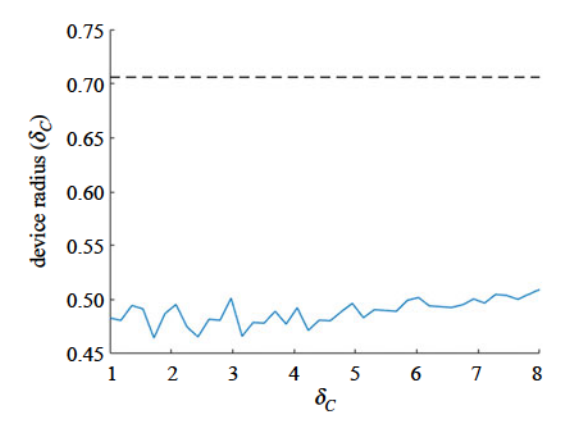


Figure 11. The solid blue curve corresponds to circular active surface radii (relative to the scaling parameter δ_C) to achieve exterior cloaking of a point source located at (10, 1) for 40 different values of the scaling parameter δ_C and for Ω centred at (10, 10) (figure 6). The dotted line corresponds to the value for which the circles touch. Since the blue data points are below the dotted line, there are gaps between the circular active surfaces, showing that even the 'extended cloaking devices' do not completely surround the object (exterior cloaking). (Online version in colour.)

This choice is not a statement of what is feasible, but simply for illustration purposes. In figure 10, we have T = 2 and $u_{max} \approx 6.2$.

To show that we are achieving exterior cloaking even when replacing the multipolar sources by extended cloaking devices (circular active surfaces), we changed the scale δ_C (radius of Ω) of the cloaking configuration in figure 6 with $\delta_D = \sqrt{2}\delta_C$, keeping Ω as a disc with a fixed centre (10,10) and a fixed point source positioned at (10,1), which generates the incident field (see also §3c(i)). For all values of δ_C , we used the same diffusivity $\sigma=1.3$ in (4.2), truncation M=22 and 128 points to discretize a parametric representation of $\partial\Omega$. The temperature fields where evaluated using 130 wavenumbers. The computation was repeated for 40 equally spaced δ_C in the interval [1,8], chosen so that the divergence region R from theorem 3.2 does not include the source location. For each δ_C , the cloak field was evaluated on a 100 × 100 uniform grid of the square $[0,20]^2$ and the circles outside of which $|\mathfrak{u}(x,t)| \leq \mathfrak{u}_{\max}$ were determined with T=1 in (4.4). We display in figure 11 the radius of these circles relative to δ_C and as a function of δ_C . The dotted line in figure 11 corresponds to the radius for which the circular active surfaces would touch and match the divergence region R. As we can see from figure 11, the circular active sources do not touch, and thus we have exterior cloaking even in this situation. Roughly speaking, according to figure 11, the 'urchins' have a radius that is about 70% of the radius of the grey circles in figure 6.

(d) From the frequency domain to the time domain

For convenience, we express the numerical algorithm we use to go from frequency domain to time domain in terms of the Laplace transform of $\mathfrak{u}(x,t)$ rather than the Fourier–Laplace transform (1.6). Under the same growth condition assumption (1.7) on $\mathfrak{u}(x,t)$, its Laplace transform is

$$u(x,s) = \int_0^\infty dt [e^{-st} u(x,t)],$$
 (4.5)

which is well defined for Re(s) > α , where $\alpha \ge 0$ is defined in §4b. Clearly we have $\mathfrak{u}(x,s) = u(x,is)$, where the right-hand side is the Fourier–Laplace transform of \mathfrak{u} given in (1.6). The inverse Laplace transform is then given by

$$u(x,t) = \frac{1}{2\pi i} \int_{c-i\infty}^{c+i\infty} ds[e^{st}u(x,s)], \tag{4.6}$$

for any $c > \alpha$.⁶ We follow the numerical method in [59] for computing the inverse Laplace transform by approximating it with a discrete Fourier transform (or DFT, which can be evaluated efficiently with the Fast Fourier Transform or FFT, see [60] for a definition). For a review of numerical inverse Laplace transform methods, see [61]. The idea is that to a uniform grid of the time interval [0,T] with N points, i.e. $t_p = p\Delta t \in [0,T]$, $p=0,\ldots,N-1$, $\Delta t = T/N$, we associate the discretization of a dual variable w given by $w_q = q\Delta w$, $q=0,\ldots,N-1$, $\Delta w = 2\pi/T$. The discretizations are chosen such that $t_pw_q = 2\pi pq/N$, which is the negative of the phase of the complex exponential in the DFT of length N. Using the change of variables s=c+iw in equation (4.6) and approximating with a Riemann sum on a finite interval yields the following (we assume u(x,t) is real)

$$\begin{split} \mathbf{u}(x,t) &= \frac{1}{2\pi} \int_{-\infty}^{\infty} \mathrm{d}w [\exp(ct) \exp(\mathrm{i}wt) \mathbf{u}(x,c+\mathrm{i}w)] \\ &\approx \frac{1}{2\pi} \sum_{q=-(N-1)}^{N-1} \Delta w [\exp(ct) \exp(\mathrm{i}w_q t) \mathbf{u}(x,c+\mathrm{i}w_q)] \\ &= \frac{\exp(ct)}{T} \sum_{q=-(N-1)}^{N-1} [\exp(\mathrm{i}w_q t) \mathbf{u}(x,c+\mathrm{i}w_q)] \\ &= 2 \frac{\exp(ct)}{T} \mathrm{Re} \left[\sum_{q=0}^{N-1} [\exp(-\mathrm{i}w_q t) \mathbf{u}(x,c-\mathrm{i}w_q)] - \frac{\mathbf{u}(x,c)}{2} \right], \end{split}$$

where the last equality follows by the symmetry for Laplace transforms of real functions ($\overline{u(x,s)} = u(x,\overline{s})$). By evaluating at the t_v , our approximation can be written in terms of the real part of a DFT:

$$\mathbf{u}(x,t_p) = 2 \frac{\exp(ct_p)}{T} \operatorname{Re} \left[\sum_{q=0}^{N-1} [\exp(-\mathrm{i}t_p w_q) \mathbf{u}(x,c-\mathrm{i}w_q)] - \frac{\mathbf{u}(x,c)}{2} \right]$$
$$= 2 \frac{\exp(ct_p)}{T} \operatorname{Re} \left[\operatorname{fft}(\mathbf{u}(x,c-\mathrm{i}w_q),q=0,\ldots,N-1) - \frac{\mathbf{u}(x,c)}{2} \right].$$

Here fft(v) represents the DFT of a vector v of length N, as defined in [60]. Thus we end up evaluating the frequencies $\omega_q = w_q + \mathrm{i} c$, $q = 0, \ldots, N-1$. As noted in [59], the convergence only holds for [0,T/2), so in practice we use $\widetilde{N} = 2N+2$ and only use the first N+1 time steps to give convergence on the interval [0,T]. Here the additional two frequencies mean the terminal time step is T as opposed to $T-\Delta T$. Since the heat equation solutions we consider decay, we take $\alpha=0$ and set $c=\alpha-(\Delta w/2\pi)\ln(10^{-6})>0$. We note that there are methods to speed up convergence of this class of numerical inverse Laplace transform, e.g. [62].

5. Summary and perspectives

In our earlier work on active exterior cloaking for the parabolic heat equation [55], we noted in the concluding remarks that our approach could also be tied to the active exterior cloaking strategies for the Helmholtz equation by going to Fourier or Laplace domain in time. Here we have shown that it is possible to cloak objects from thermal measurements by using active heat sources, starting from a zero temperature condition. We believe that our work opens up a new path for active cloaking for a variety of physical situations, in addition to the class of differential equations

⁶We note that the assumptions of §4b (i.e. the growth control of the source term, the zero initial condition and the causality of u) imply that for any $\xi > \alpha \ge 0$: $e^{-\xi t}u(x,t) \in L^2([0,\infty), H^2(\mathbb{R}^2))$ and (using the heat equation) that $e^{-\xi t}\partial_t u \in L^2([0,\infty), L^2(\mathbb{R}^2))$. Thus, one has that $u(\cdot,s) = s^{-1} \mathcal{L}(\partial_t u)(\cdot,s)$ is analytic with respect to s for Re(s) ≥ α , where \mathcal{L} stands for the Laplace transform. Since $||\mathcal{L}(\partial_t u)(\cdot,s)|| \to 0$ for Re(s) ≥ $c > \alpha$ and $|s| \to \infty$, we get $||u(\cdot,s)|| = o(|s|^{-1})$. We need a little more of decay to use the formula (4.6) for the inverse Laplace transform. It is enough to assume that there exists $\varepsilon > 0$ such that $||u(\cdot,s)|| \le C|s|^{-(1+\varepsilon)}$ for Re(s) ≥ $c > \alpha$. Then, (4.6) is well defined as a Bochner integral valued in $L^2(\mathbb{R}^2)$ (see e.g. the proof of [19], Theorem 2.5.1 or [22]) and thus also pointwise for a. e. $x \in \mathbb{R}^2$ and all $t \ge 0$.

of the form (1.5). Indeed, complex wavenumbers make it possible to model pseudodifferential operators in time such as fractional time derivatives [63] and integro-differential equations. This opens new avenues in active exterior cloaking. To give an example of this flexibility, consider a (non-dimensionalized) heat equation with memory that arises when considering homogenized diffusion models in fractured media [64]

$$\frac{\partial u}{\partial t} + \int_{0}^{t} \mathfrak{p}(t-\tau) \frac{\partial u}{\partial t}(\tau) d\tau = \Delta u + \mathfrak{h}, \tag{5.1}$$

where $\mathfrak{h}(x,t)$ is a source term and $\mathfrak{p}(t)$ is a causal convex monotone decreasing history function (e.g. $\mathfrak{p}(t) = \alpha \exp[-\alpha t]$ for $t \ge 0$). Indeed by taking Fourier–Laplace transform and assuming zero-initial conditions we get in the frequency domain

$$\Delta u(x,\omega) - (-i\omega + p(\omega))u(x,\omega) = -h(x,\omega). \tag{5.2}$$

The present work allows us to also study active cloaking in the context of diffusive photon density waves governed by

$$\frac{\partial \mathfrak{u}}{\partial t} + \mu \mathfrak{u} = \sigma \Delta \mathfrak{u} + \mathfrak{h}, \quad \text{for } t > 0,$$
 (5.3)

where $\mu > 0$ is an absorption coefficient, σ is a conductivity and \mathfrak{h} represents the photon current density (photon flow per unit surface and per unit time). Making use of the Fourier–Laplace transform (1.6) and assuming zero initial conditions, (5.3) takes the form of the Helmholtz equation in the context of diffusion wave scattering

$$\Delta u(x;\omega) + \frac{\mathrm{i}\omega - \mu}{\sigma} u(x;\omega) = -\frac{h(x,\omega)}{\sigma},\tag{5.4}$$

where we note that (5.4) reduces to (4.3), when $\omega \gg \mu$. Scattering cancellation of such diffusive waves has been addressed in [65,66].

Moreover, advection-diffusion problems play a prominent role notably in diffusion and mixing of fluid flow modelled by [67]

$$\rho c \frac{\partial \mathbf{u}}{\partial t} = -\mathbf{v} \cdot \nabla \mathbf{u} + \kappa \Delta \mathbf{u} + \mathbf{h}, \text{ for } t > 0,$$
 (5.5)

where v is a constant velocity, ρ is a mass density, κ a conductivity and c the heat capacity. The same equation is known as the Fokker–Planck equation and is central to models for transport of salt, heat, buoys and markers in geophysical flows [68,69]. It turns out that one can recast (5.5) using the exponential variable transform [70]

$$u(x,t) = \exp\left[\frac{v}{2\kappa} \cdot x\right] w(x,t) \quad \text{and} \quad h(x,t) = \exp\left[\frac{v}{2\kappa} \cdot x\right] g(x,t)$$
 (5.6)

together with the Fourier-Laplace transform (1.6), into the Helmholtz equation (assuming zero initial conditions)

$$\Delta w(x;\omega) - \tau^2 w(x;\omega) = -\frac{g(x,\omega)}{\kappa},\tag{5.7}$$

where $\tau^2 = (|v|/2\kappa)^2 - i\omega/\sigma$, and $\sigma = \kappa/(\rho c)$.

Finally, the exterior cloaking theory that we developed may allow us to also achieve exterior cloaking in the context of Maxwell–Cattaneo heat waves governed by [71]

$$\tau \frac{\partial^{2} \mathfrak{u}}{\partial t^{2}} + \frac{\partial \mathfrak{u}}{\partial t} = \kappa \Delta \mathfrak{u} + \tau \sigma \Delta \frac{\partial \mathfrak{u}}{\partial t} + \mathfrak{h}, \quad \text{for } t > 0,$$
 (5.8)

where κ is the thermal conductivity, σ accounts for diffusive phenomena, τ is the thermal relaxation time (that corresponds to the time it takes for a medium to reduce its temperature to half). We assume that κ , τ , σ are positive constants. Making use of the Fourier–Laplace transform (1.6) with zero initial conditions, (5.8) takes the form of the Helmholtz equation in the context of

$$\Delta u(x;\omega) + \frac{\omega(\omega\tau + i)}{\kappa - i\omega\tau\sigma}u(x;\omega) = -\frac{h(x,\omega)}{\kappa - i\omega\tau\sigma},$$
(5.9)

and thus one can define $k^2 = \omega(\omega \tau + i)/(\kappa - i\omega \tau \sigma)$ that, unlike for the Fourier heat equation (4.3), can lead to propagating features (when Re(k^2) > 0). Scattering cancellation of such diffusive waves has been addressed in [72].

Another situation where complex wavenumbers may play a prominent role is for inplane pressure and shear elastodynamic waves propagating in passive, dissipative, active or even viscoelastic media (the case of anti-plane shear waves would be covered by the twodimensional scalar Helmholtz equation with complex wavenumber). The latter, viscoelastic media, would require using the Helmholtz decomposition proposed in [73] $u = \nabla \Phi + \nabla \times \Psi$, with Ψ a divergence free vector field, in the vector Navier equation

$$(\tilde{\lambda} + 2\tilde{\mu})\nabla\nabla \cdot u + \tilde{\mu}\nabla^2 u + \rho\omega^2 u = 0, \tag{5.10}$$

where $\tilde{\lambda} = \lambda + \eta_p \mathfrak{M}$, $\tilde{\mu} = \mu + \eta_s \mathfrak{M}$, \mathfrak{M} being a convolution operator with certain power law (named after Szabo & Wu [74]), λ , μ are the usual Lamé parameters, ρ is the density and η_s , $\eta_p \ll 1$. Our approach would then be applied to Helmholtz equations with the complex wavenumbers for shear (s) and pressure (p) waves

$$k_m^2(\omega) = \omega^2 \left(1 - \frac{v_m}{c_m^2} \mathcal{M}(\omega) \right), \ m = s, \ p, \tag{5.11}$$

with $c_p = \sqrt{(\lambda + 2\mu)/\rho}$, $c_s = \sqrt{\mu/\rho}$, the pressure and shear wave velocities, respectively, $v_p = (\eta_p + 2\eta_s)/\rho$, $v_s = \eta_s/\rho$ and where the multiplication operator \mathcal{M} is the Fourier transform of the convolution operator \mathfrak{M} . The Hodge decomposition can also be applied to split the elastodynamic wave equation with isotropic viscoelasticity into two acoustic wave equations in time (P and S waves) that can be transformed into the Helmholtz equation, see [75].

There may also be ways of adapting our approach to other differential operators in space. One example would be to consider constant anisotropic media (e.g. coming from a homogenization approach). We believe that our strategy could be also applied to (1.5) wherein the Laplacian is replaced by a bi-Laplacian in the right-hand side. This problem arises when modelling flexural waves in thin elastic plates, which are governed by the Kirchhoff-Love equation. Active cloaking in this context has been considered in [9]. We are also considering applying our theory to active cloaking for flexural gravity waves in floating thin elastic plates that would involve a tri-Laplacian in the right-hand side of (1.5) [76].

We conjecture that our approach can be adapted to the three-dimensional Helmholtz equation for complex wavenumbers, which would allow us to address cloaking in general dispersive media (including media with losses or gain). As in [7], we plan to use an addition theorem for the Green function involving spherical Hankel functions, e.g. ([4], §3.3). Neither the Green function nor the spherical Hankel functions have branch-cuts, which may simplify the results for complex wavenumbers. Finally, we note that open questions related to gain media (Im(k) < 0) remain. In particular what is a sensible functional space setting for the exterior Green representation formula and for the scattering problem in gain media. We believe that the approach of exterior cloaking which we have developed in this article allows us to cover a broad range of problems for active cloaking of diffusion and wave phenomena.

Data accessibility. We provide the following supplementary materials. (i) A movie animating figure 10. (ii) The MATLAB code to reproduce figures 3, 5, 7–11 is available in the repository [77].

The data are provided in the electronic supplementary material [78].

Authors' contributions. M.C.: conceptualization, formal analysis, investigation, methodology, supervision, validation, visualization, writing—original draft, writing—review and editing; T.D.: conceptualization, data curation, formal analysis, investigation, methodology, software, validation, visualization, writing—

original draft, writing—review and editing; S.G.: conceptualization, formal analysis, investigation, methodology, supervision, validation, visualization, writing—original draft, writing—review and editing;

F.G.V.: conceptualization, data curation, formal analysis, funding acquisition, investigation, methodology, project administration, resources, software, supervision, validation, visualization, writing—original draft, writing—review and editing.

All authors gave final approval for publication and agreed to be held accountable for the work performed therein.

Conflict of interest declaration. We declare we have no competing interest.

Funding. T.D. and F.G.V. were supported by the National Science Foundation (grant no. DMS-2008610).

Appendix A. Proof of lemma 2.2

Proof. Step 1: We prove first (2.9). The entire function J_n is defined ([11], eq. 10.2.2) via the following power series:

$$J_{n}(z) := \sum_{k=0}^{\infty} \frac{(-1)^{k}}{k! (n+k)!} \left(\frac{z}{2}\right)^{n+2k} = \frac{1}{n!} \left(\frac{z}{2}\right)^{n} + \sum_{k=1}^{\infty} \frac{(-1)^{k}}{k! (n+k)!} \left(\frac{z}{2}\right)^{n+2k}, \quad \forall z \in \mathbb{C}.$$
 (A 1)

As $1/(n+k)! \le 1/(n+1)!$ for $k \ge 1$, one gets

$$\left| \sum_{k=1}^{\infty} \frac{(-1)^k}{k! (n+k)!} \left(\frac{z}{2} \right)^{n+2k} \right| \le \frac{1}{(n+1)!} \left(\frac{|z|}{2} \right)^{n+2} \left[\sum_{k=1}^{\infty} \frac{1}{k!} \left(\frac{|z|}{2} \right)^{2k-2} \right] \le \frac{C_{K_1}}{(n+1)!} \left(\frac{|z|}{2} \right)^{n+2}, \quad (A2)$$

where the positive constant C_{K_1} is defined by

$$C_{K_1} = \max_{z \in K_1} f(|z|) \quad \text{with } f \text{ entire defined by } f(z) := \sum_{k=1}^{\infty} \frac{1}{k!} \left(\frac{z}{2}\right)^{2k-2}, \ \forall z \in \mathbb{C}. \tag{A 3}$$

We point out that $f(z) = 4(\exp(z^2/4) - 1)/z^2$ for $z \neq 0$ and f(0) = 1. Thus, (2.9) is an immediate consequence of (A 1) and (A 2).

Step 2: The asymptotic formula (2.10) for J'_n follows immediately from the asymptotic expansion (2.9) and the recurrence formula (see [11], eqn 10.6.1) $J'_n(z) = (1/2)(J_{n-1}(z)) - J_{n+1}(z)$). Another way to obtain the formula (2.10) is to differentiate the power series that defines J_n and apply the same method as for formula (2.9).

Step 3: We now prove (2.11). By definition of the Hankel function $H_n^{(1)}$ (see [11], eqn 10.4.3), one has for all $z \in \mathbb{C} \setminus (-\infty, 0]$:

$$H_n^{(1)}(z) + \frac{\mathrm{i}(n-1)!}{\pi} \left(\frac{2}{z}\right)^n = J_n(z) + \mathrm{i}Y_n(z) + \frac{\mathrm{i}(n-1)!}{\pi} \left(\frac{2}{z}\right)^n.$$

Using (A 1) and the series representation of Y_n on $\mathbb{C} \setminus (-\infty, 0]$ (see [11], eqn 10.8.1) on the previous expression leads to:

$$H_n^{(1)}(z) + \frac{\mathrm{i}(n-1)!}{\pi} \left(\frac{2}{z}\right)^n = -\frac{\mathrm{i}}{\pi} \left(\frac{2}{z}\right)^n \sum_{k=1}^{n-1} \frac{(n-k-1)!}{k!} \left(\frac{z}{2}\right)^{2k} + I_2(n,z),\tag{A4}$$

where

$$I_2(n,z) = \left(\frac{z}{2}\right)^n \left(\sum_{k=0}^{\infty} \left(\frac{i}{\pi} \left(2 \ln \left(\frac{z}{2}\right) - \psi(k+1) - \psi(k+n+1)\right) + 1\right) \frac{(-1)^k}{k!(n+k)!} \left(\frac{z}{2}\right)^{2k}\right)^{2k}$$

where ln is the principal value of the logarithm function with a branch cut on $(-\infty,0]$ and $\psi := \Gamma'/\Gamma$ with Γ the well-known Gamma function. We estimate now the two terms appearing in (A 4). For the first one, one obtains

$$\left| -\frac{i}{\pi} \left(\frac{2}{z} \right)^n \sum_{k=1}^{n-1} \frac{(n-k-1)!}{k!} \left(\frac{z}{2} \right)^{2k} \right| \le \frac{(n-2)!}{\pi} \left(\frac{2}{|z|} \right)^{n-2} \left[\sum_{k=1}^{n-1} \frac{1}{k!} \left(\frac{|z|}{2} \right)^{2k-2} \right].$$

$$\le \frac{C_{K_2}}{\pi} (n-2)! \left(\frac{2}{|z|} \right)^{n-2}, \tag{A5}$$

with the constant C_{K_2} defined by replacing the compact K_1 by K_2 in (A 3). As the function ψ evaluated on integers (see [11], eqn 5.4.14) is given by

$$\psi(m+1) := \sum_{p=1}^{m} \frac{1}{p} + \gamma$$
 for $m \ge 1$ with $\gamma =: \Gamma'(1) = \psi(1)$ the Euler constant,

the second term of (A4) can be bounded by

$$|I_{2}(n,z)| \leq \frac{1}{\pi} \frac{(n-2)!}{(n-2)!} \left(\frac{2}{|z|}\right)^{n-4} \left(\frac{|z|}{2}\right)^{2n-4} \times \left[\sum_{k=0}^{\infty} \left(2\left|\ln\left(\frac{z}{2}\right)\right| + C + \sum_{p=1}^{k+1} \frac{1}{p} + \sum_{p=1}^{n+k} \frac{1}{p}\right) \frac{1}{k!(n+k)!} \left(\frac{|z|}{2}\right)^{2k}\right],$$

with $C = 2\gamma + \pi$ (we point out that we use the inequality $\psi(k+1) \le \psi(k+2)$ for $k \ge 0$ to avoid the particularity of the case k = 0). Then, using the following inequality $\sum_{p=1}^{m} 1/p \le \ln(m) + 1$ for $m \ge 1$ (obtained by comparison of the harmonic series with the integral) and the fact that $\ln(k+1) \le \ln(n+k)$, one gets that

$$\begin{split} |I_2(n,z)| &\leq \frac{1}{\pi} \frac{(n-2)!}{(n-2)!} \left(\frac{2}{|z|}\right)^{n-2} \left(\frac{|z|}{2}\right)^{2n-2} \\ &\times \left[\sum_{k=0}^{\infty} \left(2\left|\ln\left(\frac{z}{2}\right)\right| + C + 2\ln(n+k) + 2\right) \frac{1}{k!(n+k)!} \left(\frac{|z|}{2}\right)^{2k}\right]. \end{split}$$

Notice that

$$\frac{\ln(n+k)}{(n+k)!} \le \frac{\ln(n+k)}{(n+k)(n+k-1)!} \le \frac{1}{(n+k-1)!} \le \frac{1}{(k+1)!} \quad \text{and} \quad \frac{1}{(n+k)!} \le \frac{1}{(k+1)!} \text{ for } n \ge 2$$

so we obtain that

$$|I_2(n,z)| \leq \frac{1}{\pi} \frac{(n-2)!}{(n-2)!} \left(\frac{2}{|z|}\right)^{n-2} \left(\frac{|z|}{2}\right)^{2n-2} \left(2\left|\ln\left(\frac{z}{2}\right)\right| + C + 4\right) \left[\sum_{k=0}^{\infty} \frac{1}{k!(k+1)!} \left(\frac{|z|}{2}\right)^{2k}\right].$$

By introducing the entire functions,

$$g(z) = \sum_{n=2}^{\infty} \frac{1}{(n-2)!} \left(\frac{|z|}{2}\right)^{2n-2} \quad \text{and} \quad h(z) = \sum_{k=0}^{\infty} \frac{1}{k!(k+1)!} \left(\frac{z}{2}\right)^{2k}, \ \forall z \in \mathbb{C},$$

it follows that

$$|I_2(n,z)| \leq \tilde{C}_{K_2}(n-2)! \left(\frac{2}{|z|}\right)^{n-2} \quad \text{with } \tilde{C}_{K_2} = \frac{1}{\pi} \max_{K_2} g(|z|) \left(2 \left| \ln \left(\frac{z}{2}\right) \right| + C + 4\right) h(|z|).$$

References

- Kadic M, Bückmann T, Schittny R, Wegener M. 2013 Metamaterials beyond electromagnetism. Rep. Prog. Phys. 76, 126501. (doi:10.1088/0034-4885/76/12/126501)
- Guevara Vasquez F, Milton GW, Onofrei D. 2009 Active exterior cloaking for the 2D Laplace and Helmholtz equations. *Phys. Rev. Lett.* 103, 073901. (doi:10.1103/PhysRevLett.103.073901)
- 3. Kellogg OD. 1967 Foundations of potential theory. Die Grundlehren der mathematischen Wissenschaften, Band 31. Berlin, Germany: Springer. (Reprint from the first edition of 1929.)
- Colton D, Kress R. 2013 Inverse acoustic and electromagnetic scattering theory, vol. 93. Applied Mathematical Sciences, 3rd edn. New York, NY: Springer.
- Miller DAB. 2006 On perfect cloaking. Opt. Express 14, 12457–12466. (doi:10.1364/ OE.14.012457)

royalsocietypublishing.org/journal/rsta

Phil. Trans. R. Soc. A 380: 20220073

- Guevara Vasquez F, Milton GW, Onofrei D. 2011 Exterior cloaking with active sources in two dimensional acoustics. Wave Motion 48, 515–524. (doi:10.1016/j.wavemoti.2011.03.005)
- 7. Guevara Vasquez F, Milton GW, Onofrei D, Seppecher P. 2013 Transformation elastodynamics and active exterior cloaking. In *Acoustic metamaterials: Negative refraction, imaging, lensing and cloaking* (eds RV Craster, S Guenneau). Berlin, Germany: Springer.
- 8. Norris AN, Amirkulova FA, Parnell WJ. 2014 Active elastodynamic cloaking. *Math. Mech. Solids* **19**, 603–625. (doi:10.1177/1081286513479962)
- 9. O'Neill J, Selsil Ö, McPhedran R, Movchan A, Movchan N. 2015 Active cloaking of inclusions for flexural waves in thin elastic plates. *Q. J. Mech. Appl. Math.* **68**, 263–288. (doi:10.1093/qjmam/hbv007)
- 10. Onofrei D. 2014 Active manipulation of fields modeled by the Helmholtz equation. *J. Integral Equ. Appl.* **26**, 553–579. (doi:10.1216/JIE-2014-26-4-553)
- 11. DLMF 2018. NIST digital library of mathematical functions. See http://dlmf.nist.gov/, Release 1.0.21 of 15 December 2018. (eds FWJ Olver, AB Olde Daalhuis, DW Lozier, BI Schneider, RF Boisvert, CW Clark, BR Miller, BV Saunders).
- 12. Martin PA. 2006 *Multiple scattering*, vol. 107. Encyclopedia of Mathematics and its Applications. Cambridge, UK: Cambridge University Press. Interaction of time-harmonic waves with *N* obstacles.
- 13. Cassier M, Hazard C. 2013 Multiple scattering of acoustic waves by small sound-soft obstacles in two dimensions: mathematical justification of the Foldy-Lax model. *Wave Motion* **50**, 18–28. (doi:10.1016/j.wavemoti.2012.06.001)
- 14. Meng W, Wang L. 2016 Bounds for truncation errors of Graf's and Neumann's addition theorems. *Numer. Algorithms* **72**, 91–106. (doi:10.1007/s11075-015-0035-1)
- 15. Dautray R, Lions JL. 1992 *Mathematical analysis and numerical methods for science and technology*, vol. 5. Berlin, Germany: Springer. Evolution problems. I, With the collaboration of Michel Artola, Michel Cessenat and Hélène Lanchon, Translated from the French by Alan Craig.
- 16. Ockendon J, Howison S, Lacey A, Movchan A. 2003 *Applied partial differential equations*. Applied Partial Differential Equations. Oxford, UK: Oxford University Press.
- 17. Gumerov NA, Duraiswami R. 2005 Fast multipole methods for the Helmholtz equation in three dimensions. Amsterdam, The Netherlands: Elsevier.
- 18. Friedlander FG. 1998 *Introduction to the theory of distributions*, 2nd edn. Cambridge, UK: Cambridge University Press. With additional material by M. Joshi.
- 19. Arendt W, Batty CJK, Hieber M, Neubrander F. 2011 *Vector-valued Laplace transforms and Cauchy problems*, vol. 96. Basel, Switzerland: Birkhäuser.
- 20. Evans LC. 2010 *Partial differential equations*, vol. 19. Graduate Studies in Mathematics, 2nd edn. Providence, RI: American Mathematical Society.
- 21. Lions JL, Magenes E. 1972 *Non-homogeneous boundary value problems and applications*, vol. I. Die Grundlehren der mathematischen Wissenschaften, Band 181. New York, NY: Springer. (Translated from the French by P. Kenneth.)
- 22. Sayas FJ. 2016 *Retarded potentials and time domain boundary integral equations*, vol. 50. Springer Series in Computational Mathematics. Cham, Switzerland: Springer. (A road map.)
- Zemanian AH. 1972 Realizability theory for continuous linear systems. New York, NY: Academic Press.
- 24. Skaar J. 2006 Fresnel equations and the refractive index of active media. *Phys. Rev. E* **73**, 026605. (doi:10.1103/PhysRevE.73.026605)
- 25. Dyatlov S, Zworski M. 2019 *Mathematical theory of scattering resonances*, vol. 200. Graduate Studies in Mathematics. Providence, RI: American Mathematical Society.
- Kresin GI, Maz'ya VG. 1993 Criteria for validity of the maximum modulus principle for solutions of linear strongly elliptic second order systems. *Potential Anal.* 2, 73–99. (doi:10.1007/BF01047674)
- 27. Krutitskii PA. 1998 The Dirichlet problem for the dissipative Helmholtz equation in a plane domain bounded by closed and open curves. *Hiroshima Math. J.* **28**, 149–168. (doi:10.32917/hmj/1206126877)
- 28. Tip A. 1998 Linear absorptive dielectrics. *Phys. Rev. A* 57, 4818. (doi:10.1103/PhysRevA. 57.4818)
- 29. Figotin A, Schenker JH. 2005 Spectral theory of time dispersive and dissipative systems. J. Stat. Phys. 118, 199–263. (doi:10.1007/s10955-004-8783-7)

royalsocietypublishing.org/journal/rsta

Phil. Trans. R. Soc. A 380: 20220073

- 30. Gralak B, Tip A. 2010 Macroscopic Maxwell's equations and negative index materials. *J. Math. Phys.* **51**, 052902. (doi:10.1063/1.3374670)
- 31. Cassier M, Milton GW. 2017 Bounds on Herglotz functions and fundamental limits of broadband passive quasistatic cloaking. *J. Math. Phys.* **58**, 071504. (doi:10.1063/1.4989990)
- 32. Cassier M, Joly P, Kachanovska M. 2017 Mathematical models for dispersive electromagnetic waves: an overview. *Comput. Math. Appl.* **74**, 2792–2830. (doi:10.1016/j.camwa.2017. 07.025)
- 33. Bellis C, Lombard B. 2019 Simulating transient wave phenomena in acoustic metamaterials using auxiliary fields. *Wave Motion* **86**, 175–194. (doi:10.1016/j.wavemoti.2019.01.010)
- 34. Ramakrishna SA. 2005 Physics of negative refractive index materials. *Rep. Prog. Phys.* **68**, 449. (doi:10.1088/0034-4885/68/2/R06)
- 35. DiSalvo FJ. 1999 Thermoelectric cooling and power generation. *Science* **285**, 703–706. (doi:10.1126/science.285.5428.703)
- 36. Norris AN, Amirkulova FA, Parnell WJ. 2012 Source amplitudes for active exterior cloaking. *Inverse Problems* 28, 105002. (doi:10.1088/0266-5611/28/10/105002)
- Colton D, Kress R. 2013 Integral equation methods in scattering theory, vol. 72. Classics in Applied Mathematics. Philadelphia, PA: Society for Industrial and Applied Mathematics (SIAM). Reprint of the 1983 original [MR0700400].
- 38. McLean W. 2000 Strongly elliptic systems and boundary integral equations. Cambridge, UK: Cambridge University Press.
- 39. Nédélec JC. 2001 *Acoustic and electromagnetic equations*, vol. 144. Applied Mathematical Sciences. New York, NY: Springer. (Integral representations for harmonic problems.)
- 40. Hao S, Barnett AH, Martinsson PG, Young P. 2014 High-order accurate methods for Nyström discretization of integral equations on smooth curves in the plane. *Adv. Comput. Math.* **40**, 245–272. (doi:10.1007/s10444-013-9306-3)
- 41. Kapur S, Rokhlin V. 1997 High-order corrected trapezoidal quadrature rules for singular functions. SIAM J. Numer. Anal. 34, 1331–1356. (doi:10.1137/S0036142995287847)
- 42. Guenneau S, Amra C, Veynante D. 2012 Transformation thermodynamics: cloaking and concentrating heat flux. *Opt. Express* **20**, 8207–8218. (doi:10.1364/OE.20.008207)
- 43. Greenleaf A, Lassas M, Uhlmann G. 2003 Anisotropic conductivities that cannot be detected by EIT. *Physiol. Meas.* 24, 413. (doi:10.1088/0967-3334/24/2/353)
- 44. Pendry JB, Schurig D, Smith DR. 2006 Controlling electromagnetic fields. *Science* 312, 1780–1782. (doi:10.1126/science.1125907)
- 45. Petiteau D, Guenneau S, Bellieud M, Zerrad M, Amra C. 2014 Spectral effectiveness of engineered thermal cloaks in the frequency regime. *Sci. Rep.* 4, 1–9. (doi:10.1038/srep07386)
- 46. Schittny R, Kadic M, Guenneau S, Wegener M. 2013 Experiments on transformation thermodynamics: molding the flow of heat. *Phys. Rev. Lett.* **110**, 195901. (doi:10.1103/PhysRevLett.110.195901)
- 47. Narayana S, Sato Y. 2012 Heat flux manipulation with engineered thermal materials. *Phys. Rev. Lett.* **108**, 214303. (doi:10.1103/PhysRevLett.108.214303)
- 48. Xu H, Shi X, Gao F, Sun H, Zhang B. 2014 Ultrathin three-dimensional thermal cloak. *Phys. Rev. Lett.* **112**, 054301. (doi:10.1103/PhysRevLett.112.054301)
- 49. Han T, Bai X, Gao D, Thong JT, Li B, Qiu CW. 2014 Experimental demonstration of a bilayer thermal cloak. *Phys. Rev. Lett.* **112**, 054302. (doi:10.1103/PhysRevLett.112.054302)
- 50. Hu R, Zhou S, Li Y, Lei DY, Luo X, Qiu CW. 2018 Illusion thermotics. *Adv. Mater.* **30**, 1707237. (doi:10.1002/adma.201707237)
- 51. Alwakil A, Zerrad M, Bellieud M, Amra C. 2017 Inverse heat mimicking of given objects. *Sci. Rep.* 7, 1–17. (doi:10.1038/srep43288)
- 52. Diatta A, Guenneau S. 2010 Non-singular cloaks allow mimesis. *J. Opt.* **13**, 024012. (doi:10.1088/2040-8978/13/2/024012)
- Nguyen DM, Xu H, Zhang Y, Zhang B. 2015 Active thermal cloak. *Appl. Phys. Lett.* 107, 121901. (doi:10.1063/1.4930989)
- 54. Huang X, Liu Y, Tian Y, Zhang W, Duan Y, Ming T, Xu G. 2020 A thermal cloak with thermoelectric devices to manipulate a temperature field within a wide range of conductivity ratios. *J. Phys. D: Appl. Phys.* **53**, 115502. (doi:10.1088/1361-6463/ab60ee)
- 55. Cassier M, DeGiovanni T, Guenneau S, Guevara Vasquez F. 2021 Active thermal cloaking and mimicking. *Proc. R. Soc. A* 477, 20200941. (doi:10.1098/rspa.2020.0941)

royalsocietypublishing.org/journal/rsta

Phil. Trans. R. Soc. A 380: 20220073

- 56. Xu L, Yang S, Huang J. 2019 Dipole-assisted thermotics: experimental demonstration of dipole-driven thermal invisibility. *Phys. Rev. E* **100**, 062108. (doi:10.1103/PhysRevE. 100.062108)
- 57. Sinigaglia C, Quadrelli DE, Manzoni A, Braghin F. 2022 Fast active thermal cloaking through PDE-constrained optimization and reduced-order modelling. *Proc. R. Soc. A* 478, 20210813. (doi:10.1098/rspa.2021.0813)
- 58. Costabel M. 1990 Boundary integral operators for the heat equation. *Integral Equ. Oper. Theory* **13**, 498–552. (doi:10.1007/BF01210400)
- 59. Hsu J, Dranoff J. 1987 Numerical inversion of certain Laplace transforms by the direct application of fast Fourier transform (FFT) algorithm. *Comput. Chem. Eng.* **11**, 101–110. (doi:10.1016/0098-1354(87)80011-X)
- 60. Frigo M, Johnson S. 2005 The Design and Implementation of FFTW3. *Proc. IEEE* **93**, 216–231. (doi:10.1109/JPROC.2004.840301)
- 61. Cohen AM. 2007 *Numerical methods for Laplace transform inversion*, vol. 5. Numerical Methods and Algorithms. New York, NY: Springer.
- 62. Brančík L. 2002 Matlab oriented matrix laplace transforms inversion for distributed systems simulation. In *Proc. of 12th Int. Scientific Conf. Radioelektronika* 2002, p. 114. Department of Radio and Electronics, FEI STU Bratislava, Slovak Republic.
- 63. Podlubny I. 1999 Fractional differential equations, vo. 6. San Diego, CA: Academic Press.
- 64. Hornung U, Showalter RE. 1990 Diffusion models for fractured media. *J. Math. Anal. Appl.* **147**, 69–80. (doi:10.1016/0022-247X(90)90385-S)
- 65. Schittny R, Kadic M, Bückmann T, Wegener M. 2014 Invisibility cloaking in a diffusive light scattering medium. *Science* **345**, 427–429. (doi:10.1126/science.1254524)
- 66. Farhat M, Chen PY, Guenneau S, Bağcı H, Salama KN, Alu A. 2016 Cloaking through cancellation of diffusive wave scattering. *Proc. R. Soc. A* 472, 20160276. (doi:10.1098/rspa.2016.0276)
- 67. Constantin P, Kiselev A, Ryzhik L, Zlatoš A. 2008 Diffusion and mixing in fluid flow. *Ann. Math.* 168, 643–674. (doi:10.4007/annals.2008.168.643)
- 68. Murphy N, Cherkaev E, Zhu J, Xin J, Golden K. 2020 Spectral analysis and computation for homogenization of advection diffusion processes in steady flows. *J. Math. Phys.* **61**, 013102. (doi:10.1063/1.5127457)
- 69. Coti Zelati M, Pavliotis GA. 2020 Homogenization and hypocoercivity for Fokker–Planck equations driven by weakly compressible shear flows. *IMA J. Appl. Math.* **85**, 951–979. (doi:10.1093/imamat/hxaa035)
- 70. Li B, Evans J. 1991 Boundary element solution of heat convection-diffusion problems. *J. Comput. Phys.* **93**, 255–272. (doi:10.1016/0021-9991(91)90181-J)
- 71. Joseph DD, Preziosi L. 1989 Heat waves. *Rev. Mod. Phys.* **61**, 41–73. (doi:10.1103/RevModPhys.61.41)
- 72. Farhat M, Guenneau S, Chen PY, Alù A, Salama KN. 2019 Scattering cancellation-based cloaking for the Maxwell-Cattaneo heat waves. *Phys. Rev. Appl.* 11, 044089. (doi:10.1103/PhysRevApplied.11.044089)
- 73. Bretin E, Bustos LG, Wahab A. 2011 On the Green function in visco-elastic media obeying a frequency power-law. *Math. Methods Appl. Sci.* **34**, 819–830. (doi:10.1002/mma.1404)
- 74. Szabo TL, Wu J. 2000 A model for longitudinal and shear wave propagation in viscoelastic media. J. Acoust. Soc. Am. 107, 2437–2446. (doi:10.1121/1.428630)
- 75. Albella Martínez J, Imperiale S, Joly P, Rodríguez J. 2018 Solving 2D linear isotropic elastodynamics by means of scalar potentials: a new challenge for finite elements. *J. Sci. Comput.* 77, 1832–1873. (doi:10.1007/s10915-018-0768-9)
- 76. Farhat M, Chen PY, Bagci H, Salama KN, Alù A, Guenneau S. 2020 Scattering theory and cancellation of gravity-flexural waves of floating plates. *Phys. Rev. B* **101**, 014307. (doi:10.1103/PhysRevB.101.014307)
- 77. Cassier M, Degiovanni T, Guenneau S, Guevara Vasquez F. 2021 Code to generate figures in 'Active exterior cloaking for the two-dimensional Helmholtz equation with complex wavenumbers and application to thermal cloaking'. See https://github.com/fguevaravas/code_AEC.
- 78. Cassier M, DeGiovanni T, Guenneau S, Guevara Vasquez F. 2022 Active exterior cloaking for the two-dimensional Helmholtz equation with complex wavenumbers and application to thermal cloaking. Figshare. (doi:10.6084/m9.figshare.c.6167566)